CZECH TECHNICAL UNIVERSITY IN PRAGUE

Faculty of Nuclear Sciences and Physical Engineering

Department of Physics

The influence of structure functions uncertainties on the kinematic characteristics of Z boson created in proton-proton collisions at $\sqrt{s} = 14$ TeV

Research project

Miroslav Myška

Supervisor: RNDr. Pavel Staroba, CSc., Institute of Physics, Academy of Sciences of the Czech Republic Prague

Academic year 2005/2006

Contents

Chapter 1

Introduction

Future experiments at LHC(Large Hadron Collider) at CERN will enable to test Standard Model predictions in new kinematic area. For the correct interpretation of measured data it is necessary to investigate the influence of all possible sources of uncertainty: the theoretical one, uncertainty arising from detector effects and background. The aim of this work is to estimate the influence of the uncertainty of our knowlege of parton distribution functions of the proton on the kinematic distributions of the Z boson.

For the purpose of this study I use the nomenclature "Drell-Yan Z boson". I mean by this Z boson created by quark-antiquark pair annihilation. The decay channel $Z \rightarrow e^+ + e^-$ is investigated. The basic kinematic relations characterising deep inelastic scattering (DIS) and Drell-Yan pair creation are described in Chapter 3.

The formalism used for the description of elastic and inelastic lepton-proton collisons is reported in the next chapter. Parton model is presented in Chapter 5. The analytical formula for differential cross section of Drell-Yan Z production is described in Chapter 6. The most important experiments measuring proton structure functions are summarized in Chapter 7.

The main part of this work is the analysis of events $pp \rightarrow X + Z \rightarrow e^- e^+$ generated by two programms commonly used in particle physics - Herwig [19] and Pythia [20]. Five sets of events (differing only by parton distribution function) were generated by Herwig. Two classes of comparisons are presented. The first one is the comparison of distributions of kinematic quantities of the Z boson events generated with Herwig and Pythia. The second one is the comparison of events generated by Herwig with different parton distribution functions.

The natural unit system is applied in the whole study. Planck constant and speed of light is considered as one. The following conversion relations can be used to recompute the values of quantities in both directions:

$$1 \text{ kg} = 5.609589206\ 10^{26} \text{ GeV}$$
$$1 \text{ s} = 1.5192676\ 10^{24} \text{ GeV}^{-1}$$
$$1 \text{ m} = 5.06773122\ 10^{15} \text{ GeV}^{-1}.$$

Chapter 2

Quick overview of additive quark model

Standard model consists of two substantial theories : quantum chromodynamics (QCD) and GWS theory of electroweak interaction.

Quark model was suggested by two physicists independently in January 1964: Murray Gell-Mann and his student George Zweig. According to their idea, all hadrons are made up of a small variety of more basic entities, called quarks, bound together in different ways. In their work were used only three lightest quarks: u, d, s and we will follow these historical steps.

All multiplets can be built from the fundamental representation of the group SU(3), so called "flavor SU(3) symmetry", which is violated by low mass differences among u, d, s. Each quark is assigned spin $1/2\ \hbar$ and baryon number $B = 1/3$. Baryons are made of three quarks (qqq) and the mesons of a quark-antiquark pair ($q\bar{q}$). The new additive quantum number is shown as the hypercharge $Y = B + S$, rather than the strangeness S. The electrical charge Qe is $Q = I_3 + Y/2$. Baryon conservation means it is impossible to destroy or to make a single quark, but it is permitted annihilate or create a quark-antiquark pair only.

One problem arised soon in this theory. For example, a Δ^{++} is described by the symmetric wave function $u \uparrow u \uparrow u \uparrow$, whereas it is expected antisymmetry under the exchange of identical fermions. The explanation is that the quarks possess an additional attribute, called colour, which can take three possible values: R, G, or B. All hadrons are postulated to be colourless. They belong to the singlet representations of the SU(3) colour group. The required antisymmetric character of the total wavefunction is achieved. It is overall

symmetric in space, spin and flavor structure and antisymmetric in colour.

The discovery in November 1974 of a very narrow resonance, called J/ψ particle, followed later by the appearance of a second narrow resonance, ψ', can rightly be called the "November revolution". The ψ and ψ' were immediately interpreted as the lowest bound states of a new quark called charm and its antiquark, $c\bar{c}$. New additive quantum number C = ± 1 is assigned to the c quark and antiquark, respectively. The value of this quantum number is zero for all other quarks. The c quark has charge $Q = +2/3$ and isospin I = 0. The relation for hypercharge is updated to $Y = B + S + C$.

The model was changed even twice by discovery of quark b and t with new quantum numbers called beauty and true. In 1977 series of narrow resonances were discovered in p-p experiments at Fermilab. The lowest resonance, now called Υ (upsilon), was considered as analogous of J/ψ like a bound state of new quark called b and its antiquark $\bar{b}$. The b quark has charge $Q = -1/3$ and its high mass violates the flavor SU(5) very much.

The theory expected a quark partner to the b, signed t, with a charge $Q = +2/3$. Its existence was confirmed in 1995. Due to its properties the flavor symmetry SU(6) isn't considered. On the other hand the SU(3) colour symmetry is regarded as exact.

Chapter 3

Kinematics

3.1 Differential cross section

A calculational scheme is implemented by summing the relevant Feynman diagrams that can be drawn for the process under study. Feynman developed his rules using the machinery of quantum field theory from an appropriate Lagrangian. This approach has the practical advantage that we can calculate transition rates and cross sections in relatively simple way.

The differential cross section for the general process $1+2 \rightarrow 3+4+...n$ in the center-of-mass frame is given by simple equation [1]

$$d\sigma = \frac{(2\pi)^4}{|\vec{v_1} - \vec{v_2}|} \frac{1}{2E_1} \frac{1}{2E_2} |M|^2 \prod_{i=3}^{n} \frac{d\vec{p_i}}{(2\pi)^3 2E_i} \delta^4(p_1 + p_2 - \sum_{i=3}^{n} p_i), \tag{3.1}$$

where $d\Omega$ is the element of solid angle about $\vec{p_3}$, $s = (E_1 + E_2)^2$, $|\vec{p_1}| = |\vec{p_2}| = p_i$ and $|\vec{p_3}| = |\vec{p_4}| = ... = p_f$.

The technique of Feynman diagrams enables in principle to calculate the invariant amplitude M in any order of the relevant coupling constant. Before turning to the parton structure functions, it is important to master basic kinematics relevant for further consideration.

3.2 Deep inelastic scattering

We assume the "neutral current" process, namely when ingoing lepton is the same as outgoing. These processes can be mediated by the exchange of

either the photon or the neutral vector boson Z. The latter contribution is dominant for really high energies, but in kinematic range of DIS it can be neglected.

The e-p scattering in the leading order is shown in Fig. 3.1. More detailed elements of proton structure can be resolved by increasing the transferred momentum $-q^2$ of the photon. The transferred four-momentum squared

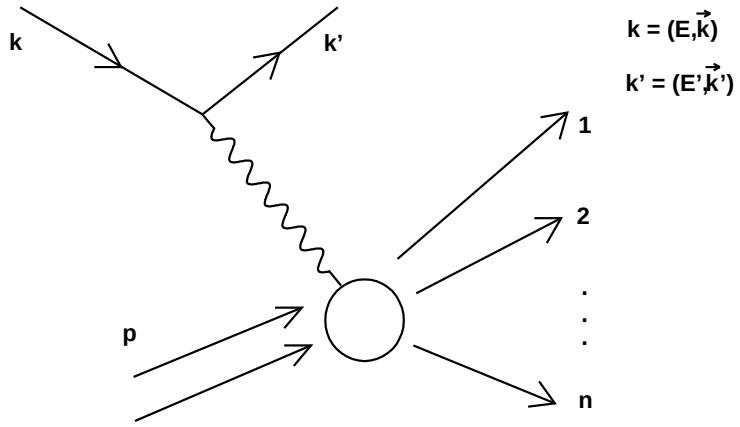

Figure 3.1: The lowest - order diagram for inclusive e-p deep inelastic scattering. k^2 is neglected in relativistic limit, $p^2 = M^2$ is mass squared of the proton.

is negative in the relativistic approach: $q^2 < 0$. The proof is based on the definition of $q = (\nu, \vec{q}) = k - k'$ and on relativistic limit, where $|\vec{k}|^2 = E^2$ and $|\vec{k'}|^2 = E'^2$, Θ is electron scattering angle in nucleon rest frame with respect to the electron beam direction and ν is the electron energy loss:

$$\begin{aligned} q^2 = \nu^2 - |\vec{q}|^2 = (E' - E)^2 - (|\vec{k}|^2 + |\vec{k'}|^2 - 2|\vec{k}||\vec{k'}|\cos\Theta) = \\ = E'^2 - 2EE' + E^2 - |\vec{k}|^2 - |\vec{k'}|^2 + 2|\vec{k}||\vec{k'}|\cos\Theta = \\ = -2EE' + 2EE'\cos\Theta = -2EE'(1 - \cos\Theta) \leq 0. \end{aligned} \tag{3.2}$$

The proton will often break up into complicated multiparticle states with large invariant mass W. If the final state of proton is described with four-momentum P as a sum over all momenta of fragments, we will get $P^2 = W^2$. From momentum conservation follows $W^2 = (p+q)^2$.

Two independent variables can describe the inelastic process. The following set of variables is commonly used:

$$Q^2 = -q^2 = -(k-k')^2 = 2kk' = -2EE'(1-\cos\Theta) = 4EE'\sin^2(\Theta/2),$$

$$\nu = (p.q)/m = E - E', \tag{3.3}$$

$$x = Q^2/(2p.q) = Q^2/(2M\nu),$$
$$y = (p.q)/(p.k) = \nu/E.$$

In standard notation the pairs $(\nu, q^2), (x, y)$ or (x, Q^2) are most often used to uniquely specify the state of the scattered electron and to write down the cross section provided that colliding particles are unpolarized.

It is possible to express other quantities in new variables. E.g. total CMS energy squared:

$$s = (k+p)^2 = M^2 + 2kp = M(2E+M) = M^2 + Q^2/(xy) \tag{3.4}$$

and invariant mass of the hadronic system:

$$W^2 = (p+q)^2 = Q^2(1-x)/x + M^2 = 2M\nu - Q^2 + M^2. \tag{3.5}$$

Notice, all quantities defined above are relativistic invariant.

The term "deep inelastic scattering" means that both invariants Q^2 and pq are large with respect to M

$$Q^2 \gg M^2, \quad \nu \gg M.$$

The so called Bjorken limit corresponds to the idealized case when $Q^2 \to \infty$, $pq \to \infty$ but the ratio x remains finite.

3.3 Drell-Yan process

Deep inelastic scattering is investigated by colliding electrons with a proton beam. From these experiments information about nucleon structure functions can be extracted. To determine the internal structure of other hadrons

different method has to be used - collision of two hadrons as hard as possible. The process most similar to deep inelastic scattering in these reactions is the annihilation of a quark and an antiquark, each deriving from a different hadron, into a lepton pair. This is called the Drell - Yan process. Our task is investigation of the special channel, when quark-antiquark pair annihilates into Z boson and electron - positron pair is created. The process is schematically shown in Fig. 3.2.

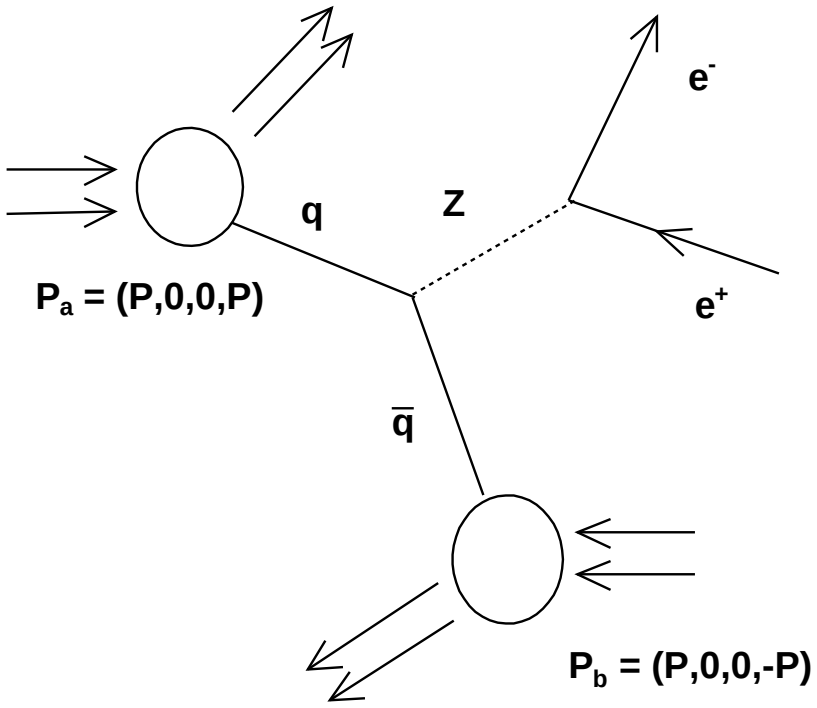

Figure 3.2: Schematic view of the creation of the Drell - Yan Z boson in the p-p interaction.

Here a designates the first and b the second hadron, thus x_a and x_b give the momentum fraction carrying by corresponding parton (quark). It means that x,y $\in$ (0,1). Both quarks in Fig.3.2 have to be of the same flavor and colour.

Notice, that it it assumed the head-on collision of two hadrons with non-zero momentum only in z-axis direction. Consequently Z has the transverse momentum equal to zero. The non-zero p_t of the Drell - Yan Z is generated just by radiation of gluons - see Fig.3.3.

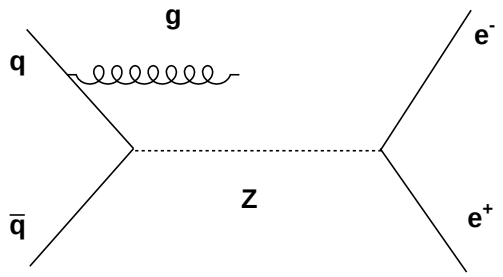

Figure 3.3: Drell - Yan process with Z in next to leading order.

Kinematic difference between Drell -Yan and deep inelastic scattering is that now is $q^2 > 0$ in comparison with $q^2 = -Q^2 < 0$ for DIS. It is clear that $q^2 = M^2$ holds with M the invariant mass of the leptonic pair. The running coupling constant still has its usual form with $\alpha(Q^2) \to \alpha(M^2)$.

The invariant mass of the colliding protons is

$$s = (P_a + P_b)^2. \tag{3.6}$$

The momentum of the partons participating in the Drell - Yan process expressed in terms of fractions $x_a,\ x_b$ are

$$p_a = x_a\ P_a, \qquad p_b = x_b\ P_b. \tag{3.7}$$

Neglecting hadron and quark masses, the invariant mass of the lepton pair is then

$$M^2 = (p_a + p_b)^2 = 2p_a\ p_b = 2x_a\ x_b\ P_a\ P_b = x_a\ x_b\ (P_a + P_b)^2 = x_a\ x_b\ s \tag{3.8}$$

and is equal to four-momentum of intermediate Z squared. It is standard to express from this equation product of x_a and x_b and define a new variable

$$\tau = x_a\ x_b = (M^2)/s. \tag{3.9}$$

In the CMS of the lepton pair it is possible to express the rapidity of the Z boson by the following formula:

$$y = \frac{1}{2} \ln \left(\frac{E + P_L}{E - P_L} \right) = \frac{1}{2} \ln \left(\frac{x_a}{x_b} \right), \tag{3.10}$$

where $P_L = x_a \; E_a - x_b \; E_b$.
Using new variables it is possible to write the fractional momenta x_a and x_b as

$$x_a = e^y \; Q/\sqrt{s}, \quad x_b = e^{-y} \; Q/\sqrt{s}. \tag{3.11}$$

Chapter 4

Structure of the proton

In this chapter is discussed scattering on proton. Such ranges of energy are regarded, that it is essential to involve gradually more detailed theory of structure of hadrons. From now it is impossible to consider the proton as a point-like particle. Generally, this theory develops different levels of structure functions.

4.1 Elastic scattering of electron on point-like proton

At the beginning of investigation of inner structure of proton it is useful to transform the DIS kinematics (Chapter 3) into the laboratory frame. These results can be then directly applied to electron-quark scattering. For now the goal is to find the cross section of elastic lepton-proton scattering for the case of point-like proton. In the lowest order of perturbative quantum electrodynamics this process is described by photon exchange diagram in Fig. 4.1.

Using the Dirac formalism and Feynman rules the invariant amplitude is given by

$$M = -e^2 \bar{u}(k', s_4)\gamma^\mu u(k, s_2)\frac{1}{q^2}\bar{u}(p', s_3)\gamma_\mu u(p, s_1). \tag{4.1}$$

To obtain the unpolarized cross section, the square of the matrix element M has to be summed over the spins s_3, s_4 of the final and averaged over the

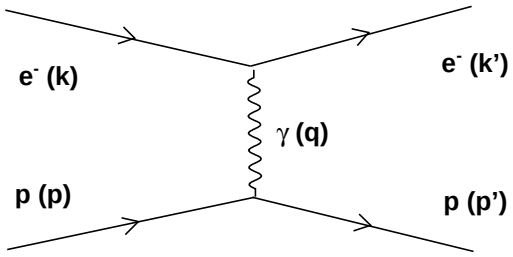

Figure 4.1: The LO diagram for e-p elastic scattering. The low energetic photon interract with the whole proton due to its long wavelength.

spins s_1, s_2 of the initial fermions [1]

$$\overline{|M|^2} = \frac{8e^4}{q^4} 2M^2 E' E \Big(\cos^2 \frac{\Theta}{2} - \frac{q^2}{2M^2} \sin^2 \frac{\Theta}{2} \Big). \tag{4.2}$$

The first kinematic relation from (3.3) was used for the derivation of this formula. The final result (4.3) is reached by inserting (4.2) into (3.1), where the electron mass is neglected and dE' integration is performed

$$\frac{d\sigma}{d\Omega}\Big|_{lab} = \Big(\frac{\alpha^2}{4E^2 \sin^4 \frac{\Theta}{2}} \Big) \frac{E'}{E} \Big\{ \cos^2 \frac{\Theta}{2} - \frac{q^2}{2M^2} \sin^2 \frac{\Theta}{2} \Big\}, \tag{4.3}$$

where the factor

$$\frac{E'}{E} = \frac{1}{1 + \frac{2E}{M} \sin^2 \frac{\Theta}{2}}. \tag{4.4}$$

Returning to (4.2), it is convenient to separate the sums over the electron and proton spins and to write $\overline{|M|^2}$ as a contraction of two tensors

$$\overline{|M|^2} = \frac{e^4}{q^4} L^{(1)\mu\nu} L^{(2)}_{\mu\nu}. \tag{4.5}$$

These tensors can be calculated by well-established trace technique, which is described in many publications. Thus the tensor associated e.g. with the electron vertex is

$$L^{\mu\nu}_e = \frac{1}{2} \sum_{e \ spins} [\bar{u}(k') \gamma^\mu u(k)] \, [\bar{u}(k') \gamma^\nu u(k)]^*, \tag{4.6}$$

$$L_e^{\mu\nu} = \frac{1}{2} Tr\Big((\hat{k}' + m)\gamma^\mu(\hat{k} + m)\gamma^\nu\Big), \tag{4.7}$$

$$L_e^{\mu\nu} = 2(k'^\mu k^\nu + k'^\nu k^\mu - (k' \cdot k - m^2)q^{\mu\nu}). \tag{4.8}$$

This type of notation will be useful in next chapters for generalization from lepton tensor to hadron tensor.

4.2 Proton form factors

For the real proton the situation is more complicated because the strong interaction modify the point-like coupling in transition current

$$j^\mu = -e\bar{u}(k')\gamma^\mu u(k)e^{i(k'-k)\cdot x}. \tag{4.9}$$

This simple coupling has to be replaced with a structure, compatible with gauge and Lorentz invariance and parity conservation. Thus, this most general four-vector form can be constructed from p, p', q and the Dirac γ-matrices sandwiched between $\bar{u}$ and u. There are only two independent terms, γ^μ and $i\sigma^{\mu\nu}g_\nu$ that are functions of only one independent scalar variable q^2, where

$$\sigma^{\mu\nu} = \tfrac{i}{2}[\gamma^\mu\gamma^\nu - \gamma^\nu\gamma^\mu].$$

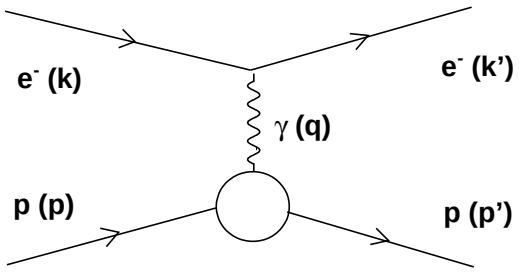

Figure 4.2: Electron proton elastic scattering. Structure of proton is described by elastic form factors dependent on q^2.

Therefore, a new transition current is connected with outer lines of proton in Fig. 4.2.

$$J^{\mu} = e\bar{u}(p')\Big[F_1(q^2)\gamma^{\mu} + \frac{\kappa}{2M}F_2(q^2)i\sigma^{\mu\nu}g_{\nu}\Big]u(p), \tag{4.10}$$

The $F_1(q^2)$ and $F_2(q^2)$ are two independent elastic electromagnetic form factors of the proton and parametrize our ignorance of the detailed structure of the proton. κ is anomalous magnetic moment. The proton is effectively seen as a particle of charge e and magnetic moment $(1+\kappa)e/2M$. For the proton was measured $\kappa = 1.793$ [1]. In the case of point-like proton where $q^2 \to 0$ is $\kappa = 0$ and the form factors of the proton must therefore be chosen so that in this limit

$$F_1(0) = 1, \qquad F_2(0) = 1.$$

The evaluation of the differential cross section using (4.10) is

$$\frac{d\sigma}{d\Omega}\Big|_{lab} = \Big(\frac{\alpha^2}{4E^2\sin^4\frac{\Theta}{2}}\Big)\frac{E'}{E}\Big\{\Big(F_1^2 - \frac{\kappa^2 q^2}{4M^2}F_2^2\Big)\cos^2\frac{\Theta}{2} - \frac{q^2}{2M^2}(F_1+\kappa F_2)^2\sin^2\frac{\Theta}{2}\Big\}, \tag{4.11}$$

This result was derived first by Rosenbluth in 1950 and therefore this formula bears his name.

Instead of F_1, F_2, it is convenient to introduce their special linear combinations G_E and G_M, called electric and magnetic form factors

$$G_E = F_1 + \frac{\kappa q^2}{4M^2}F_2, \tag{4.12}$$

$$G_M = F_1 + \kappa F_2. \tag{4.13}$$

They are defined so that no interference terms occur in the calculation of the cross section. With definition $\tau = \frac{-q^2}{4M^2}$ equation (4.11) becomes

$$\frac{d\sigma}{d\Omega}\Big|_{lab} = \Big(\frac{\alpha^2}{4E^2\sin^4\frac{\Theta}{2}}\Big)\frac{E'}{E}\Big(\frac{G_E^2 + \tau G_M^2}{1+\tau}\cos^2\frac{\Theta}{2} + 2\tau G_M^2\sin^2\frac{\theta}{2}\Big). \tag{4.14}$$

4.3 Inelastic Electron-Proton Scattering

Inelastic events in Fig.3.1, where the proton is recoiled into many final states, can not be described only by construction of general form of proton current J^μ. The expression for the invariant amplitude is directly generalized from form (4.5) to

$$\overline{|M|^2} = \frac{e^4}{q^4} L^{\mu\nu} W_{\mu\nu}, \tag{4.15}$$

where $L^{\mu\nu}$ represents the lepton tensor of (4.6) and $W_{\mu\nu}$ is hadronic tensor. Its most general form must be constructed out of the independent momenta p and q, symmetric metric tensor $g^{\mu\nu}$ and totally antisymetric Levi-Civita pseudotensor $\epsilon_{\mu\nu\alpha\beta}$

$$W_{\mu\nu}(p,q) = -W_1 g_{\mu\nu} + W_2 \tfrac{p_\mu p_\nu}{M^2} + iW_3 \epsilon_{\mu\nu\alpha\beta} p_\alpha q_\beta$$

$$+W_4 q_\mu q_\nu + W_5(p_\mu q_\nu + p_\nu q_\mu) + iW_6(p_\mu q_\nu - p_\nu q_\mu). \tag{4.16}$$

In the above decomposition $W_i(p,q)$ are unknown functions of p and q, which depend on the internal structure of the proton. But only two of them are, however independent. When the parity conservation is true antisymmetric term vanished by $W_3(p,q) = 0$ and gauge invariance, expressed as the condition

$$q^\mu W_{\mu\nu} = [-W_1 + W_4 q^2 + W_5(pq)]q_\nu + [W_2 \frac{pq}{M^2} + W_5 q^2]p_\nu + iW_6[(pq)q_\nu - q^2 p_\nu] = 0 \tag{4.17}$$

leads to three relations

$$W_6(p,q) = 0, \tag{4.18}$$

$$W_5(p,q) = -W_2(p,q)\frac{pq}{q^2 M^2}, \tag{4.19}$$

$$W_4(p,q) = W_1(p,q)\frac{1}{q^2} + W_2(p,q)\frac{(pq)^2}{q^4 M^2}. \tag{4.20}$$

This properties make the possibility to simplify (4.16) to [1]

$$W_{\mu\nu}(p,q) = -W_1(p,q)\Big(g_{\mu\nu} - \frac{q_\mu q_\nu}{q^2}\Big) + \frac{W_2(p,q)}{M^2}\Big(p_\mu - \frac{pq}{q^2}q_\mu\Big)\Big(p_\nu - \frac{pq}{q^2}q_\nu\Big). \tag{4.21}$$

So, for ep $\to$ eX in the laboratory frame we have

$$(L^e)^{\mu\nu}W_{\mu\nu} = 4EE'\Big[\cos^2\frac{\Theta}{2}W_2(\nu,q^2) + \sin^2\frac{\Theta}{2}2W_1(\nu,q^2)\Big]. \tag{4.22}$$

Instead of W_1, W_2 it is common to introduce another pair of functions

$$F_1 = M\ W_1, \qquad F_2 = \nu\ W_2. \tag{4.23}$$

The double differential cross section written in three equivalent ways different in the choice of pair of variables is

$$\frac{d\sigma}{dE'd\Omega}\Big|_{lab} = \frac{\alpha^2}{4E^2\sin^4\frac{\Theta}{2}}\Big[W_2(\nu,q^2)\cos^2\frac{\Theta}{2} + 2W_1(\nu,q^2)\sin^2\frac{\Theta}{2}\Big], \tag{4.24}$$

$$\frac{d\sigma}{dxdy} = \frac{4\pi\alpha^2(2kp)}{Q^4}\Big[\Big(1-y-\frac{M^2xy}{s}\Big)F_2(x,Q^2) + \frac{1}{2}y^2 2xF_1(x,Q^2)\Big], \tag{4.25}$$

$$\frac{d\sigma}{dxdQ2} = \frac{4\pi\alpha^2}{Q^4}\Big[\Big(1-y-\frac{M^2xy}{s}\Big)\frac{F_2(x,Q^2)}{x} + \frac{1}{2}y^2 2F_1(x,Q^2)\Big]. \tag{4.26}$$

The unknown functions $F_i(x,Q^2)$, or equivalently, $W_i(x,q^2)$ are called inelastic electromagnetic form factors or structure functions of the proton.

These cross sections were calculated for the case of the exchange of unpolarized virtual photon. Now it is possible to transfer the problem on scattering by a real photon with energy ν and polarization ϵ off the unpolarized proton. The total cross section for photon with helicity λ is

$$\sigma_\lambda^{tot} = \frac{4\pi^2\alpha}{K}\epsilon_\lambda^{\mu *}\epsilon_\lambda^{\nu}W_{\mu\nu}. \tag{4.27}$$

Using expression (4.16) for $W_{\mu\nu}$ the transverse and longitudinal cross sections are

$$\sigma_T = \frac{4\pi^2\alpha}{K}W_1(\nu,q^2), \tag{4.28}$$

$$\sigma_L = \frac{4\pi^2\alpha}{K}\Big[\Big(1-\frac{\nu^2}{q^2}\Big)W_2(\nu,q^2) - W_1(\nu,q^2)\Big], \tag{4.29}$$

where K satisfy

$$K = \frac{W^2-M^2}{2M} = \nu + \frac{q^2}{2M}. \tag{4.30}$$

Chapter 5

Introduction to parton model

5.1 Basic ideas of parton model

The parton model develops an experimental fact, that such complex system like proton starts for really small wavelength scattering to behave like a free Dirac particle, see Fig. 5.1.

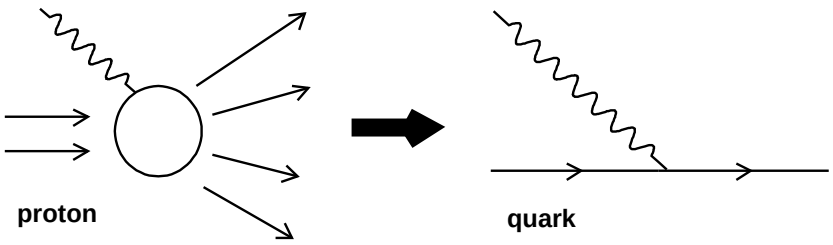

Figure 5.1: The electromagnetic interaction between electron and photon behave for sufficiently small wavelengths of virtual photons like couppling a photon with point-like charge - charged parton.

The parton model describes the proton as a composition of many "point" partons (quarks and gluons), each carrying a different fraction x of the parent proton momentum and energy. Both the proton and its parton move along the z axis, therefore the longitudinal and transverse momenta are

	proton	**parton**
energy	E	xE
momentums	p_L = p	p_L = xp
	$p_T = 0$	$p_T = 0$
mass	M	xM

The parton momentum distribution function

$$f_i(x) = \frac{dP_i}{dx} \tag{5.1}$$

describes the probability that the struck parton i carries a fraction x of the proton momentum p. The sum over all partons (charged as well as not charged) has to creates the whole proton, therefore

$$\sum_j \int dx\ x\ f_j(x). \tag{5.2}$$

Generally, an inelastic electron-proton scattering at large Q^2 is viewed simply as elastic scattering an electron on a "free" quark within the proton. This signs, that quark model is very promising theory and that there are structureless particles inside a proton. These "point" functions now display intriguing property, that they are only functions of dimensionless ratio

$$\omega = \frac{2M\nu}{Q^2} \tag{5.3}$$

and not of Q^2 and ν independently. This property, that structure functions are independent of Q^2 at constant ω, is called the Bjorken scaling.

Therefore, it is common to redefine a structure functions for parton with momentum fraction x

$$xmW_1(\nu, Q^2) \to F_1(\omega) \to F_1(x), \tag{5.4}$$

$$\nu W_2(\nu, Q^2) \to F_2(\omega) \to F_2(x). \tag{5.5}$$

In addition to F_1, F_2 it is useful to introduce the so called longitudinal structure function

$$F_L(x, Q^2) = F_2(x, Q^2)\left(1 + \frac{4M^2x^2}{Q^2}\right) - 2xF_1(x, Q^2), \tag{5.6}$$

in terms of which the ratio of longitudinal and transversal cross section is ordinarily expressed and also measured

$$R(x,Q^2) = \frac{\sigma_L(x,Q^2)}{\sigma_T(x,Q^2)} = \frac{F_L(x,Q^2)}{2xF_1(x,Q^2)}. \tag{5.7}$$

Summing results for F_1, F_2 for fraction x over the partons making up a proton, it is obtained

$$F_2(x) = \sum_i e_i^2 x f_i(x), \tag{5.8}$$

$$F_1(x) = \frac{1}{2x} F_2(x), \tag{5.9}$$

where i sums only over the charged partons, which can interact with a photon. Delta function in expression for structure function implies $x = 1/\omega$. Using this basic idea of parton model the cross section can be expressed as follows[1]

$$\left.\frac{d\sigma}{dxdy}\right|_{ep\to eX} = \frac{2\pi\alpha^2}{Q^4} s\Big[1 + (1-y)^2\Big] \sum_i e_i^2 x f_i(x), \tag{5.10}$$

where the particle masses are neglected.

Identity (5.8) can be made more concrete by including terms from additive quark model (shortly described in Chapter 2)

$$\frac{1}{x}F_2(x) = \left(\frac{2}{3}\right)^2 [u(x) + \bar{u}(x)] + \left(\frac{1}{3}\right)^2 [d(x) + \bar{d}(x)] + \left(\frac{1}{3}\right)^2 [s(x) + \bar{s}(x)] \ \ldots \tag{5.11}$$

where $u(x)$ and $\bar{u}(x)$ are the probability distributions of u quarks and antiquarks within the proton, $d(x)$ and $\bar{d}(x)$ are the probability distributions of d quarks and antiquarks atc.

5.2 Higher orders of deep inelastic e-p scattering

The parton model in previous section completely ignores the dynamical role of neutral partons. In quark model, these constituents are gluons, carriers of the strong force. Now it is essential to allow for the possibility that quark may radiate a gluon before or after being struck by the virtual photon. This process $\gamma^* q \to qg$ is shown in Fig. 5.2.

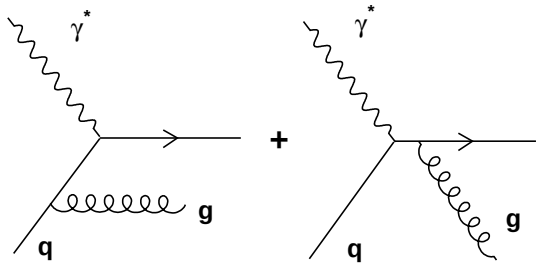

Figure 5.2: Initial- or final-state gluon radiations contribute to inclusive e-p deep inelastic scattering in O($\alpha\alpha_s$).

Moreover, a gluon participated in the proton structure can contribute to deep inelastic scattering via $\gamma^* g \to q\bar{q}$. Fig. 5.3 shows such $q\bar{q}$ pair creation. Despite of the leading order of DIS $O(\alpha)$, these processes are $O(\alpha\alpha_s)$ contributions to the cross section. The emission of gluon has two experimentally observable consequences. First, the scaling property of the structure functions will no longer be true and second, the outgoing quark will no longer be collinear with the virtual photon. These produced jets so will gain a nonzero transverse momentum p_T relative to the virtual photon.

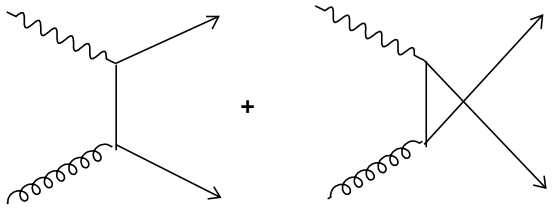

Figure 5.3: The gluon - initiated scattering contributions to inclusive e-p DIS in O($\alpha\alpha_s$).

The results for QED process $\gamma^* e \to \gamma e$ can be taken over for the calculation of invariant amplitude for process $\gamma^* q \to qg$. It can be written using

substitution $\alpha^2 \rightarrow e_i^2 \alpha \alpha_s$ as

$$\overline{|M|^2} = 32(e_i^2 \alpha \alpha_s)\frac{4}{3}\Big(- \frac{t}{s} - \frac{s}{t} + \frac{2uQ^2}{st}\Big), \tag{5.12}$$

where the factor 4/3 takes into account the summation over final and averaging over initial colours. The square of the transverse momentum of the outgoing quark, $p_T = k' \sin\Theta$, can be expressed in the limit of small-angle scattering, -t $\ll$ s, as

$$p_T^2 = \frac{s(-t)}{s + Q^2} \tag{5.13}$$

and the solid angle differential is then

$$d\Omega = \frac{4\pi}{s} dp_T^2. \tag{5.14}$$

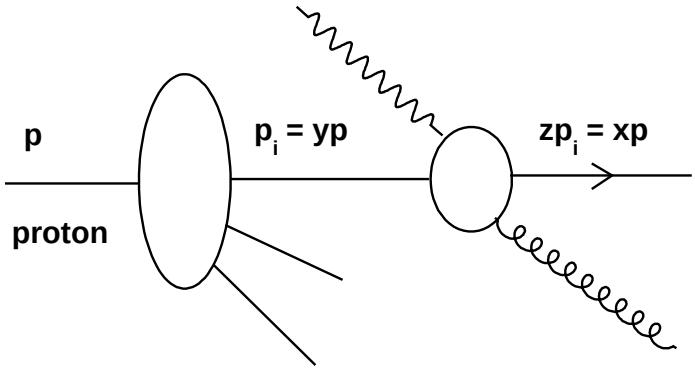

Figure 5.4: Schematic illustration of photon - parton interaction with gluon in final-state. The initial parton momentum fraction is y and final momentum fraction of that parton is x.

Using (5.13) and definition of momentum fraction z

$$z = \frac{Q^2}{2p_i q}, \tag{5.15}$$

based on kinematics in Fig. 5.4, the cross section becomes [1]

$$\frac{d\sigma}{dp_T^2} = e_i^2 \sigma_0 \frac{1}{p_T^2} \frac{\alpha_s}{2\pi} P_{qq}(z) \tag{5.16}$$

where $\sigma_0 = 4\pi^2 \alpha_s$ and

$$P_{qq}(z) = \frac{4}{3}\Big(\frac{1+z^2}{1-z}\Big) \tag{5.17}$$

represents the probability of gluon emission from quark and so becoming a quark with momentum reduced by a fraction $z = x/y$.

At high energy (s large), hence in the region -t $\ll$ s, the cross section (5.16) represents the full p_T^2 distribution of the final-state parton jets. If computed

$$\sigma(\gamma^* q \to qg) = \int_{\mu^2}^{s/4} dp_T^2 \tfrac{d\sigma}{dp_T^2} \cong e_i^2 \sigma_0 \int_{\mu^2}^{s/4} \tfrac{dp_T^2}{p_T^2} \tfrac{\alpha_s}{2\pi} P_{qq}(z)$$

$$\cong e_i^2 \sigma_0 \Big(\frac{\alpha_s}{2\pi} P_{qq}(z) \log \frac{Q^2}{\mu^2}\Big), \tag{5.18}$$

it is clearly seen, that Bjorken scaling is violated due to the presence of the $logQ^2$ factor. The structure function is directly modified to

$$\frac{F_2(x,Q^2)}{x} = \sum_q e_q^2 \int_x^1 \frac{dy}{y} q(y) \Big(\delta\Big(1-\frac{x}{y}\Big) + \frac{\alpha_s}{2\pi} P_{qq}\Big(\frac{x}{y}\Big) \log \frac{Q^2}{\mu^2}\Big), \tag{5.19}$$

where the notation for quark structure function $q(y) = f_q(y)$ have been introduced. In derivation of (5.18) the maximum p_T of the gluon

$$\Big(p_T^2\Big)_{max} = \frac{s}{4} = Q^2 \frac{1-z}{4z} \tag{5.20}$$

was used. The lower limit was set as μ in order to regularize the divergence when $p_T^2 \to 0$.

It seems very useful to absorb the $\log Q^2$ term in (5.19) into a modified quark probability distribution

$$\frac{F_2(x,Q^2)}{x} = \sum_q e_q^2 \Big(q(x) + \Delta q(x,Q^2)\Big), \tag{5.21}$$

where

$$\Delta q(x,Q^2) = \frac{\alpha_s}{2\pi} \log\Big(\frac{Q^2}{\mu^2}\Big) \int_x^1 \frac{dy}{y} q(y) P_{qq}\Big(\frac{x}{y}\Big). \tag{5.22}$$

The quark densities $q(x, Q^2)$ now depend on Q^2. By the Q^2 evolution of the quark densities it is meant an integro-diferencial equation for $q(x, Q^2)$. Such equation is called "Altarelli-Parisi evolution equation":

$$\frac{d}{d\log Q^2} q(x, q^2) = \frac{\alpha_s}{2\pi} \int_x^1 \frac{dy}{y} q(y, Q^2) P_{qq}\Big(\frac{x}{y}\Big). \tag{5.23}$$

Now the second $O(\alpha\alpha_s)$ process described in Fig. 5.3 has to be incorporated into $ep \to eX$. Similarly as for the first process, the QED Compton scattering invariant amplitude is used for computation

$$\overline{|M|^2} = 32\pi^2 (e_q^2 \alpha\alpha_s) \frac{1}{2}\Big(\frac{u}{t} + \frac{t}{u} - \frac{2sQ^2}{tu}\Big). \tag{5.24}$$

Hence, the proton structure function contains the additional contribution

$$\frac{F_2(x, Q^2)}{x} = \ldots + \sum_q e_q^2 \int_x^1 \frac{dy}{y} g(y) \frac{\alpha_s}{2\pi} P_{qg}\Big(\frac{x}{y}\Big) \log \frac{Q^2}{\mu^2} \tag{5.25}$$

Here g(y) is the gluon density in the proton and

$$P_{qg} = \frac{1}{2}\Big(z^2 + (1-z)^2\Big) \tag{5.26}$$

represents the probability, that a gluon annihilates into a $q\bar{q}$ pair. This newly created quark has a fraction momentum z. The quark evolution equation becomes

$$\frac{dq_i(x, Q^2)}{d\log Q^2} = \frac{\alpha_s}{2\pi} \int_x^1 \frac{dy}{y} \Big(q_i(y, Q^2) P_{qq}\Big(\frac{x}{y}\Big) + g(y, Q^2) P_{qg}\Big(\frac{x}{y}\Big)\Big) \tag{5.27}$$

for each quark flavor i.

Gluon evolution equation can be derived by applying of analogous arguments for quarks. It has a form

$$\frac{dg(x, Q^2)}{d\log Q^2} = \frac{\alpha_s}{2\pi} \int_x^1 \frac{dy}{y} \Big(\sum_i q_i(y, Q^2) P_{gq}\Big(\frac{x}{y}\Big) + g(y, Q^2) P_{gg}\Big(\frac{x}{y}\Big)\Big), \tag{5.28}$$

where the sum runs over quarks and antiquarks of all flavors and probability functions are

$$P_{gq}(z) = \frac{4}{3} \frac{1 + (1-z)^2}{z} \tag{5.29}$$

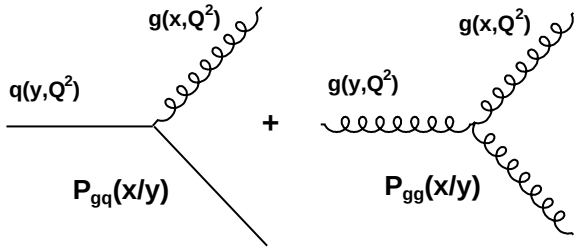

Figure 5.5: Feynman diagrams representing gluon vertices embedded in gluon structure functions.

$$P_{gg}(z) = 6\Big(\frac{1-z}{z} + \frac{z}{1-z} + z(1-z)\Big). \tag{5.30}$$

Other $O(\alpha\alpha_s)$ contributions designed in Fig. 5.6 are of the form $\delta(1-z)$ and are singular at z = 1. They must be such, that the total probability $P_{qq}(z)$ satisfies the constraint

$$\int_0^1 P_{qq}(z)dz = 0 \tag{5.31}$$

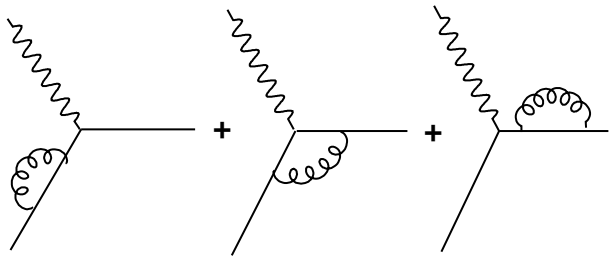

Figure 5.6: Three types of virtual gluon diagrams.

This modification of $P_{qq}(z)$ can be conveniently expressed in terms of the so-called "+ prescription" formalism. Here the term $1/(1-z)$ is replaced by $1/(1-z)_+$ due to regularization. The "+ prescription" is defined as

$$\int_0^1 dz \frac{f(z)}{(1-z)_+} = \int_0^1 dz \frac{f(z)-f(1)}{1-z}, \tag{5.32}$$

where $(1-z)_+ = (1-z)$ for $z < 1$ but is infinite at $z = 1$.

These P functions are summarily called the splitting functions. The leading order Altarelli-Parisi splitting functions are [12]

$$P_{qq}(z) = \frac{4}{3}\Big[\frac{1+z^2}{1-z}\Big]_+ = \frac{4}{3}\Big[\frac{1+z^2}{(1-z)_+}\Big] + 2\delta(1-z), \tag{5.33}$$

$$P_{qg}(z) = \frac{1}{2}\Big[z^2 + (1-z)^2\Big], \tag{5.34}$$

$$P_{gq}(z) = \frac{4}{3}\Big[\frac{1+(1-z)^2}{z}\Big], \tag{5.35}$$

$$P_{gg}(z) = 6\Big[\frac{1-z}{z} + z(1-z) + \frac{z}{(1-z)_+}\Big] + \Big[\frac{11}{2} - \frac{n_f}{3}\Big]\delta(1-z), \tag{5.36}$$

where n_f is the number of (active) quark flavors.

Chapter 6

Cross section of the Drell-Yan Z boson production

Kinematics of Drell-Yan process is described in Section 3.3. Drell-Yan process has played an important role in determining the structure functions together with e^-e^+ annihilation and deep inelastic leptoproduction. These processes serve as a test of the parton model and its QCD corrections. Just vector boson production is one of the most intensively investigated topics at both Tevatron and the LHC.

The differential cross section of the Drell-Yan Z boson production can be calculated in the lowest order of the perturbation theory by carrying over the results of deep inelastic scattering to the Drell-Yan processas as [5]

$$d\sigma_{DY} = \Big[f_a(x_a, Q^2)\cdot\bar{f}_b(x_b, Q^2)+\bar{f}_a(x_a, Q^2)\cdot f_b(x_b, Q^2)\Big]\times\sigma^{Born}(q\bar{q}\to Z)dx_a dx_b. \tag{6.1}$$

σ^{Born} is elementary cross section for annihilation of a pair quark and antiquark of invariant mass Q into a vector boson Z at the Born level.

When the σ_{DY} was measured, it turned out that the experimental cross section exceed the prediction by a factor of about 2. This missing factor is termed the "K factor" [5]. To gain a deeper understanding of the problems in Drell-Yan reactions, it is essential to incorporate first-order gluonic corrections to the annihilation graph $q + \bar{q} \to Z$, see Fig. 3.3. These gluon radiations from the initial state then generate the nonzero $p_T = Q_T$ of the Z boson. One can continue by pursing this tedious calculation order by order, but the problem of the perturbation theory is, that the cross section

$d\sigma/dQ^2dQ_T^2$ contains a term proportional to $\ln^{2n}(Q^2/Q_T^2)$ and in $Q_T \ll Q$ region diverge at every fixed power n of the α_s [6].

These large logarithms can be removed by the resummation technique. This idea is based on possibility to itterate some types of corrections into geometric or exponential series and then summed up them. The standard procedure of resummation is leading-logarithm approximation(LLA), connected with definition of Sudakov form factor $S(\Theta)$ [5]. This function express the probability that after n-gluon emissions the outgoing quark still has a scattering angle $p_T/p_{||} < \Theta$, with p_T and $p_{||}$ being defined with respect to the jet axis, or the original quark momentum, respectively.

Similar method of resummation for the Drell-Yan production was used first by Dokshitzer, Diakonov and Troyan [7]. They showed in Q_T space, that dominant contributions in the region of small Q_T can be resummed into a Sudakov form factor by double leading-logarithm approximation(DLLA). The disadvantage of this method is, that some subleading logarithms can be resummed only in the b-space, which is a Fourier conjugate of the Q_T space. b is called impact parameter. The b-space resummation method was introduced by Parisi and Petronzio [8]

In the framework of improved b-space resummation, Collins, Soper and Sterman derived a formalism for the transverse momentum distributions of vector boson production in hadronic collisions [9]. This formalism is often called the CSS formalism.

According to this formalism can be obtained the expansion for the final cross section:

$$\frac{d\sigma(p_a+p_b\to Z)}{dQ^2dydQ_T^2}=\frac{1}{2S}\sum_q\sigma^{Born}(q\bar{q}\to Z)\sum_c\sum_d\int_0^\infty bdbJ^0(Q_T,b)$$

$$\times e^{-S(b^*,Q)}e^{-S_{NP}(b,Q)}\int_{x_a}^1\int_{x_b}^1\frac{d\xi_a d\xi_b}{\xi_a\xi_b}C_{q/c}(\xi_a,b^*,\alpha_s(\frac{b_0}{b^*}))\cdot C_{\bar{q}/d}(\xi_b,b^*,\alpha_s(\frac{b_0}{b^*}))$$
$$\times f_{c/p}(x_a/\xi_a,b_0/b^*)\cdot f_{d/p}(x_b/\xi_b,b_0/b^*)$$
$$+$$
$$\sum_{n=1}^\infty\Big(\frac{\alpha_s(\mu)}{\pi}\Big)^n\Big(\frac{4\pi^4\alpha_{EM}^2}{3S}\Big)\sum_{a,b}\int_{x_a}^1\int_{x_b}^1\frac{d\xi_a d\xi_b}{\xi_a\xi_b}f_{a/p}(\xi_a,\mu)f_{b/p}(\xi_b,\mu)$$
$$\times R^{(n)}_{ab\to Z}(Q_T,Q,x_a/\xi_a,x_b/\xi_b;\mu). \qquad (6.2)$$

The first term of the sum is important in the region $Q_T \ll Q$, the second term is regular part negligible for small Q_T but important for $Q_T \sim Q$. Here, $b^* = \frac{b}{\sqrt{1+b^2/b_{max}^2}} \leq b_{max} = 0.5GeV^{-1}$ is the boundary between perturbative and nonperturbative region. The first summation in the first part is over all quark flavors, the second and third over all partons. The Sudakov form factor $S(b^*,Q)$, Wilson coefficient functions $C_{q/c}(\xi_a,b^*,\alpha_s(\frac{b_0}{b^*}))$ and functions $R^{(n)}_{ab\to Z}(Q_T,Q,x_a/\xi_a,x_b/\xi_b;\mu)$ are perturbatively calculable.

The only input to CSS formula not calculable from the principles are the nonperturbative Sudakov function $S_{NP}(b,Q)$ and the conventional parton distribution functions $f_{q/p}(x_a,\mu)$. The nonperturbative form factor $S_{NP}(b,Q)$ is determined by fitting the experimental data. Several parametrization exist. The CSS formalism well describes all the Drell-Yan data up to the Tevatron.

Chapter 7

Experiments

7.1 Electron scattering with proton target

Up to now only several experiments aimed measuring the structure functions of proton. This challenging task can be performed only by the greatest accelerating centres in the world, which can produce high energetic collisions and have a precision detection apparatus at disposal. For this purpose leptons were soon recognized as the best probes of protons because of their well-understood electromagnetic interactions.

The first e-p scattering experiments were systematically used by a group led by Robert Hofstadter at Stanford University from 1955 for the investigation of the structure of individual nucleons. These investigations with static proton target and electron beam of energies from 200 MeV up to 1 GeV earned Hofstadter the Nobel prize for physics in 1961.

In 1967, new electron linear accelerator was built in Stanford Linear Accelerator Centre (SLAC) with electron beam energy up to 20 GeV. The first serious study of deep inelastic e-p scattering was started by the group of experimentalists from SLAC and MIT (Massachusetts Institute of Technology). They discovered that proton contained tiny scattering centres. This was the first evidence of point-like charged structures in the proton and support for newly formulated quark model. A new type of physics opened up: DIS. These first MIT-SLAC results attracted the attention of Feynman who developed the basic ideas of the parton model (1968).

After that, physicist tried to probe deeper and deeper into depths of the proton. Generally, the extraction of the structure functions was based on the

measurements of double differential cross section $d\sigma/dxdQ^2$ of deep inelastic lepton-hadron scattering. Each experiment has its own kinematic range of Bjorken variable x and transferred momentum squared Q^2 as well as the type of probing lepton.

A series of eight other experiments at SLAC collected data during the years 1970 and 1985. They provided detailed knowledge of deep inelastic e-p scattering cross section. Structure functions $F_2(x, Q^2)$ and the radio $R(x, Q^2)$ were determined by the fitting procedure for all precise measurements over the entire SLAC kinematic range $0.06 \leq \mathrm{x} \leq 0.9$ and $0.6 \leq Q^2 \leq 30.0$ $(\mathrm{GeV})^2$ [12].

7.2 Muon scattering with proton target

In the next stage of proton structure investigation, more energetic lepton beams were necessary. It was difficult to produce such high-energy electron beams because of their energy losses through synchrotron radiations. Thus, muons became a natural choice as high-energy massive lepton probes with sufficient lifetime. In the following experiments, the muon beam was a tertiary beam obtained from the decay of charged pions and kaons, which in turn were obtained from the interaction of primary protons.

In the European Centre of Nuclear Research (CERN), several experiments were running in 1978-1985 under BCDMS (Bologna-CERN-Dubna-Munich-Saclay) Collaboration [22] and New Muon Collaboration (NMC) in 1986 - 1989. Data for these measurements of the proton structure function F_2 and the ratio R were collected at CERN SPS with static liquid-hydrogen target and muon beam with the highest energy of 280 GeV. BCDMC Collaboration provided a high statistics measurements with high Q^2 (7 - 260 $(\mathrm{GeV})^2$) and covered range of Bjorken variable $0.06 \leq \mathrm{x} \leq 0.8$. Analysis of the structure function was based on 1.81 10^6 reconstructed events after all cuts [13]. NM Collaboration measured inclusive deep inelastic μ-p cross sections in the kinematic range $0.002 \leq \mathrm{x} \leq 0.6$ and $0.5 \leq Q^2 \leq 75$ $(\mathrm{GeV/c})^2$. The ratio of the longitudinally and transversally polarized virtual photon absorption cross section, R, was measured for $0.002 \leq \mathrm{x} \leq 0.120$ and $1.0 \leq Q^2 \leq 25$ $(\mathrm{GeV})^2$. The full NMC data set consists of 0.54 10^6 events from the small angle trigger and 1.82 10^6 events from the large angle trigger [15].

The aim of another experiment signed Experiment 665 at Fermi National Laboratory in Batavia was to measure proton structure function $F_2(x, Q^2)$

in fixed-target inelastic muon scattering. Data were taken during the years 1987 - 1992 excluding 1989 when the detector was being upgraded. Total number of events was 159 853. The highest energy of muon beam was 470 GeV and these are the first precise measurements of $F_2(x, Q^2)$ in the low x (0.0008-0.6) and Q^2 (0.2-75 (GeV)^2) range of the data [16].

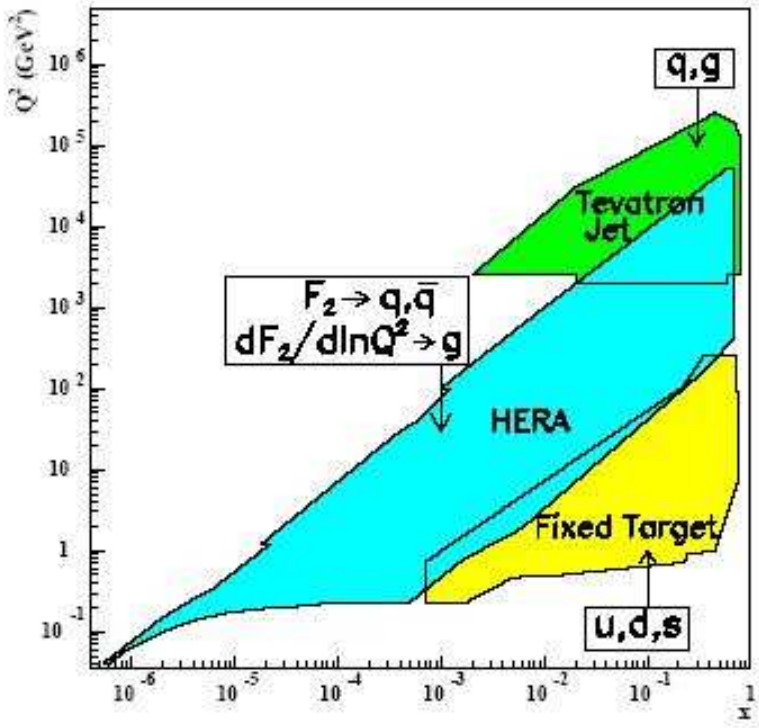

Figure 7.1: Ranges of kinematic variables x and Q^2 accessible to experiments realized up to now [2].

7.3 Positron-proton collisions

The second way, how to obtain collisions of protons with leptons at high energy was colliding. Such arrangement was possible to gain at the Hadron Electron Ring Accelerator (HERA) at Deutsches Electronen Synchrotron (DESY). At HERA, colliding particles were positrons with maximal energy

of 27.6 GeV and protons with energy of 820 GeV. The total CMS energy was $\sqrt{s} = 300.9$ GeV. In the years 1996 - 1997, two collaborations measured deep inelastic e^+-p cross sections at H1 detector and ZEUS detector, respectively. The ZEUS Collaboration [14] measured proton structure function $F_2(x, Q^2)$ in the kinematic range $10^{-5} \leq \mathrm{x} \leq 0.65$ and $2.7 \leq Q^2 \leq 30\,000$ $(\mathrm{GeV})^2$ at integrated luminosity of 30 pb^{-1}. The H1 Collaboration [18] measured $F_2(x, Q^2)$ as well as $F_L(x, Q^2)$, which was extracted using the partial derivative of the reduced cross section $(\delta\sigma_r/\delta \ln y)_{Q^2}$. The measurements covered the range $3\ 10^{-5} \leq \mathrm{x} \leq 0.2$ and $1.5 \leq Q^2 \leq 150$ $(\mathrm{GeV})^2$ and was running at integral luminosity of 20 pb^{-1}. Using low x H1 data was possible to determine the gluon distribution $xg(x, Q^2)$.

In 1999 - 2000, after accelerator upgrading, the H1 Collaboration continued with data collecting [17]. This time the energy of proton beam was 920 GeV, corresponding CMS energy rised at $\sqrt{s}$=319 GeV and integrated luminosity rised at 65.2 pb^{-1}. Collaboration provided high Q^2 measurement of F_L and $\mathrm{x}\tilde{F}_3$ in kinematic range $0.0013 \leq \mathrm{x} \leq 0.65$ and $100 \leq Q^2 \leq 30\,000$ $(\mathrm{GeV})^2$. Thus, data together with H1 low Q^2 precision data were used to perform new NLO QCD analyses in the framework of the Standard Model to extract flower separated parton distributions in the proton.

Table 7.1: Most important experiments measuring structure functions up to now.

	years	**x**	Q^2 **[(GeV)^2]**	**str. func.**
SLAC	1970-1985	6 10^{-2} - 0.90	0.6-30.0	F_2, R
BCDMS	1978-1985	6 10^{-2} - 0.80	7-260	F_2, R
NMC	1986-1989	2 10^{-3} - 0.60	0.5-75	F_2
		2 10^{-3} - 0.12	0.2-150	R
E665	1987-1992	8 10^{-4} - 0.60	0.2-75	F_2
H1	1996-1997	3 10^{-5} - 0.20	1.5-150	F_2, F_L
H1	1999-2000	1.3 10^{-2} - 0.65	100-30000	F_L, x$\tilde{F}_3$
ZEUS	1996-1997	6 10^{-5} - 0.65	2.7-30000	F_2

	events or int. lum.	**process**
SLAC		e(20GeV) + p
BCDMS	1.81 10^6	μ(280GeV) + p
NMC	2.36 10^6	μ(280GeV) + p
E665	159 853	μ(470GeV) + p
H1	20 pb^{-1}	e$^+$(27.6GeV) + p(820GeV), $\sqrt{s} = 300.9GeV$
H1	65 pb^{-1}	e$^+$(27.6GeV) + p(920GeV), $\sqrt{s} = 319.9GeV$
ZEUS	30 pb^{-1}	e$^+$(27.6GeV) + p(820GeV), $\sqrt{s} = 300.9GeV$

Chapter 8

Analysis of generated events

The main research projects measuring proton structure functions were described in Chapter 7. On the basis of these and other experiments many parametrizations of proton PDFs were prepared. The aim of this chapter is to designate their different predictions for distributions of kinematic characteristics of Z boson and its secondaries created in Drell-Yan process as well as to try to quantify their uncertainties. It will be examined generated sets of events for five different PDFs (see below) in proton-proton interactions at 14 TeV in CMS. The second aim is to compare the results for two different generators: Herwig/Jimmy and Pythia.

8.1 Monte Carlo event generators

Monte Carlo event generators for high-energy processes were evolved in order to model interactions of different particles and to predict the values of kinematic quantities observed in real experiments. The programmes provide simulations of lepton-lepton, lepton-hadron and hadron-hadron scattering.

Herwig and Pythia are general-purpose event generators based on different models of fragmentation mechanism comprehensively described in their manuals. In Pythia it is Lund's string model of hadronization [11] and in Herwig it is Cluster model of hadronization [10].

The typical high-energy event is described by an event generator simply as follows: a pair of incoming beam particles are characterized by two sets of parton distributions, which define the partonic substructure in terms of flavor composition and energy sharing. Each of an incident beam hadrons

can radiate time-like partons and so starts off building up an initial-state shower.

One parton from each of the two initial showers collides and participates in hard QCD subprocess. This can be described by exactly computed matrix elements in lowest order of perturbation theory. The nature of this hard subprocess determines the main characteristics of the event. The outgoing partons may create a similar shower (final-state shower) like ingoing partons.

In addition to the hard process many semihard or soft QCD processes, such as diffractive and elastic scattering and minimum-bias events, occur between the other partons of two incoming showers. These processes take place at low momentum transfer scale, for which the strong coupling α_s is large. Perturbation theory is not applicable and some phenomenological model has to be used. In addition hadronization process, which combine the not observable outgoing gluons and quarks into hadrons, is non-perturbative process.

8.2 Files used for the analysis

Versions of the generators used for this analysis were HERWIG 6.507 [19] together with JIMMY Version 4.0 and PYTHIA 6.323 [20]. The full matrix element (including Z, γ and interference term) was used during the generation. The minimum mass of the generated Z was set to the 60 GeV. Such steering parameters were chosen, so that programmes generated inclusive collisions with unpolarized proton-proton at c. m. energy 14 TeV in initial state and the final state contained pair electron-positron, created in Drell-Yan annihilation of the pair quark-antiquark. The programs were used in the framework ATHENA of offline software Rel 11.0.41 of the experiment ATLAS [23].

The Les Houches Accord Parton Density Function (LHAPDF) Version 4.0 interface package [21] was used for implementation of sets of PDFs into generation. Many of PDF sets are contained in this library. Five of them were chosen for this study. They are listed in Table 9.1 together with their codes and appropriate ranges for x and Q^2.

PDF set CTEQ6ll was used for the comparison between Herwig and Pythia. The main task, kinematic predictions for Z boson, was fulfilled by creation of below shown distributions of kinematic characteristics for Z and secondary electrons and positrons. Distributions of mass, transverse

Table 8.1: Proton PDFs selected for comparison.

PDF set	**code**	$\mathbf{x}_{min}$	$\mathbf{x}_{max}$	$\mathbf{Q}^2_{min}$	$\mathbf{Q}^2_{max}$
CTEQ6L	10041	10^{-6}	1	1.69	10^8
CTEQ6ll	10042	10^{-6}	1	1.69	10^8
CTEQ6m	10050	10^{-6}	1	1.69	10^8
MRST2004	20400	10^{-5}	1	1.25	10^7
ZEUS2005	60300	10^{-6}	1	0.3	2×10^5

momentum, rapidity and parton fraction momentum x_a were created.

8.3 Event selection, cuts, objects

Three aggregates of events were defined for each generated set. No cut was used for the definition of the level 1 aggregate. It is formed by all events of the corresponding set. There are 10^6 events in each level 1 aggregate.

The level 2 aggregates were created by the application of cuts to the secondary leptons. Events were accepted if electron or positron has $p_T > 20$ GeV and $|\eta| < 2.5$. So, we can distinguish electron and positron level 2 aggregates.

The level 3 aggregate contains only events in which both secondary leptons survived the lepton cut. So, it is identical to the intersection of electron and positron aggregates of level 2.

In the following text the three above defined aggregates are often mentioned as data levels. The level 3 aggregate is sometimes mentioned as Z cut.

The kinematic quantities of three types of objects are investigated in the rest of this chapter. By electrons and positrons are meant the Z secondaries obtained directly from the generator record. Generated Z corresponds to the Z from the generator record. By decayed Z is meant Z constructed from the fourmomenta of its secondaries.

The generated sets were analyzed by object oriented data analysis framework ROOT [24].

Table 8.2: Summarization of the cross sections of Z production and of decay Z after cut for all selected PDFs for Pythia and Herwig generators.

	number of generated Z	**cross section of Z production [fb]**	**Relative fraction [%]**
Pythia			
CTEQ6ll	1,000,000	$1.681\ 10^6$	100.6
Herwig			
CTEQ6ll	1,000,000	$1.671\ 10^6 \pm 948.2$	100.0
CTEQ6L	1,000,000	$1.560\ 10^6 \pm 888.2$	93.4
CTEQ6m	1,000,000	$1.701\ 10^6 \pm 955.2$	101.8
MRST2004	1,000,000	$1.731\ 10^6 \pm 982.6$	103.6
ZEUS2005	1,000,000	$1.753\ 10^6 \pm 986.2$	104.9

	number of decayed Z after cut	**cross section of decayed Z after cut [fb]**	**Relative fraction [%]**
Pythia			
CTEQ6ll	396,677	$0.667\ 10^6$	103.1
Herwig			
CTEQ6ll	387,457	$0.647\ 10^6$	100.0
CTEQ6L	386,739	$0.603\ 10^6$	93.2
CTEQ6m	407,347	$0.693\ 10^6$	107.1
MRST2004	410,713	$0.711\ 10^6$	109.9
ZEUS2005	407,654	$0.714\ 10^6$	110.4

	number of expected Z for detection	**cross section of Z detection [fb]**
Pythia		
CTEQ6ll	194,372	$0.327\ 10^6$
Herwig		
CTEQ6ll	189,854	$0.317\ 10^6$
CTEQ6L	189,502	$0.296\ 10^6$
CTEQ6m	199,600	$0.340\ 10^6$
MRST2004	201,249	$0.348\ 10^6$
ZEUS2005	199,750	$0.350\ 10^6$

8.4 Expected multiplicities of the Drell-Yan Z boson

Table 8.2 summarizes numbers of Z and cross sections for first and third level of data. It is possible to provide prediction for cross section of Z detection (last column in Table 8.2). The efficiency of lepton detection is supposed to be 70%. Neither other detector effects, nor background corrections are taken into account in this estimate. The PDF set ZEUS2005 embodies the most interesting properties. Via the final-state radiation by secondary leptons is cross section for decaying of Z reduced with respect to the large cross section of Z production.

Notice the increased relative fractions after Z cuts for all PDFs except CTEQ6L, that decreased. Especially, it is interesting to compare differences between Pythia and Herwig. In the following it will be shown that the main difference in p_T distribution, see Fig. 8.9, is responsible for differences in the cross section evolutions.

Cross sections in Table 8.2 are scatched in Fig. 8.1. This dependence of cross sections on PDFs is responsible for different normalization of following kinematic distributions.

8.5 P_T and η distributions for the Drell-Yan Z secondaries

There is a comparison of p_T distributions between Herwig and Pythia for both electrons and positrons in all three levels of data in Fig. 8.3. Notice that there are small difference between Herwig and Pythia in normalization decreased after cuts. The influence of the lepton cut can be perfectly seen at 20 GeV of p_T. There is no remarkable difference between electrons and positrons.

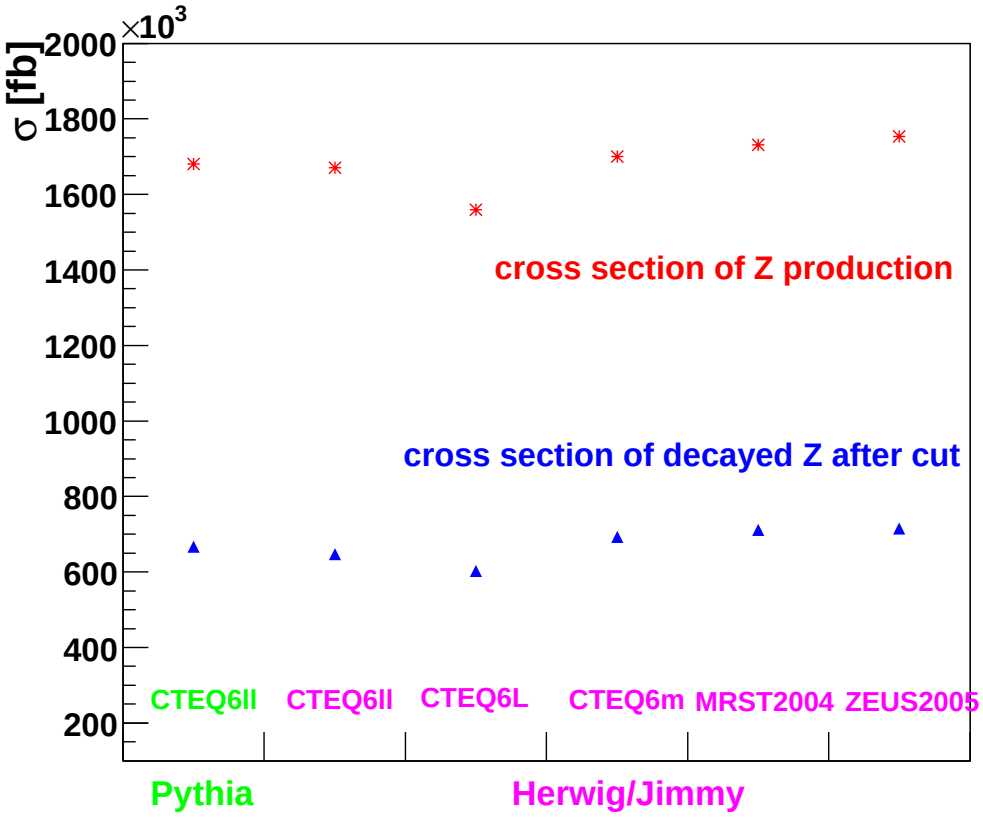

Figure 8.1: Graphical comparison of the cross sections for Drell-Yan production of Z boson. The upper red set of points corresponds to generated cross sections and the lower set corresponds to the cross section of decayed Z after cut.

In Fig. 8.4 is shown the comparison of p_T distributions for electrons after Z cut among different PDFs for Herwig generator. Distributions differ only in normalization, see Fig. 8.1, not in shape. Distributions are roughly identical for MRST2004 and ZEUS2005 PDF sets.

There is a distinct difference between Herwig and Pythia generators in Fig. 8.5, which survived all cuts. Herwig distributions are significantly wider. The effect of $|\eta| <$ cut can be well seen. The last cut causes significant change

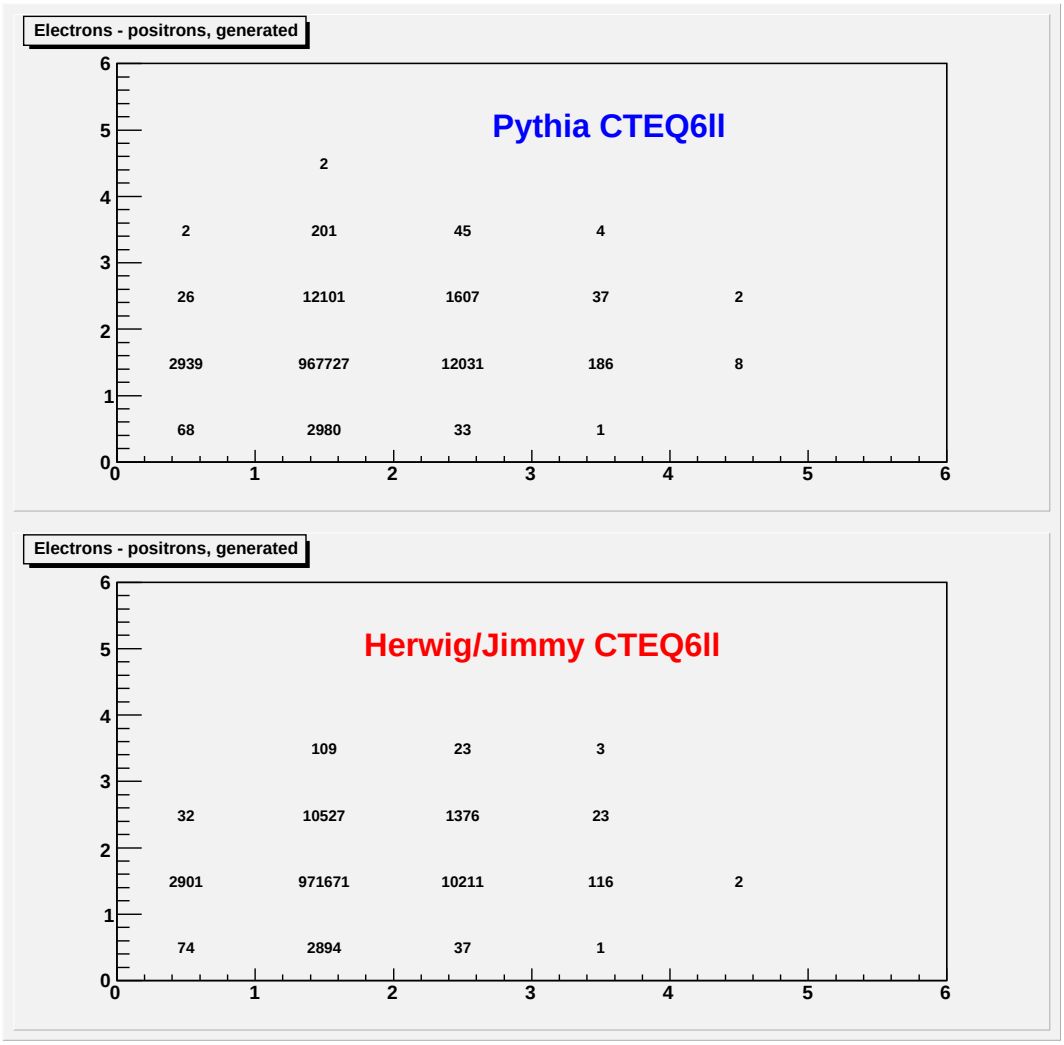

Figure 8.2: Numbers of generated electrons and positrons for events generated via Pythia and via Herwig/Jimmy. The CTEQ6ll parton distribution function is used . Numbers of electrons (x axis) and positrons (y axis) are roughly symmetric. Maximum number is 4 for both of generators.

in the shape of distribution.

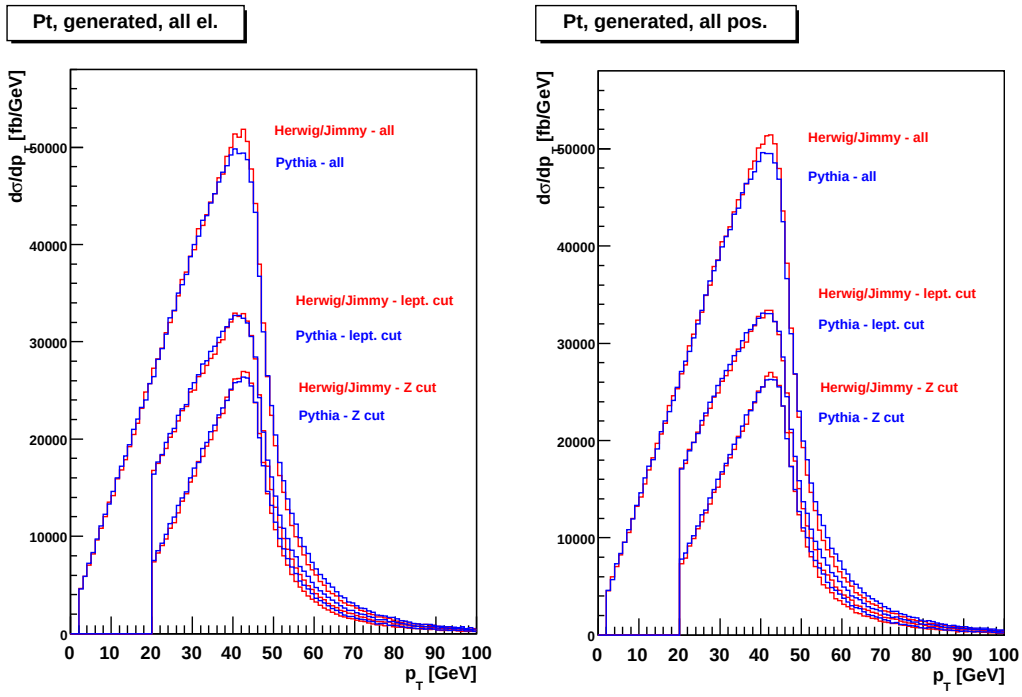

Figure 8.3: Differential cross section as a function of transverse momentum of electrons (on the left) and positrons (on the right). CTEQ6ll parton distribution function was used for both generators. Distributions are similar except normalizations and cuts.

The pseudorapidity distributions of electron are shown in Fig. 9.6 for five PDFs. The only difference is in normalization (see Fig. 9.1)

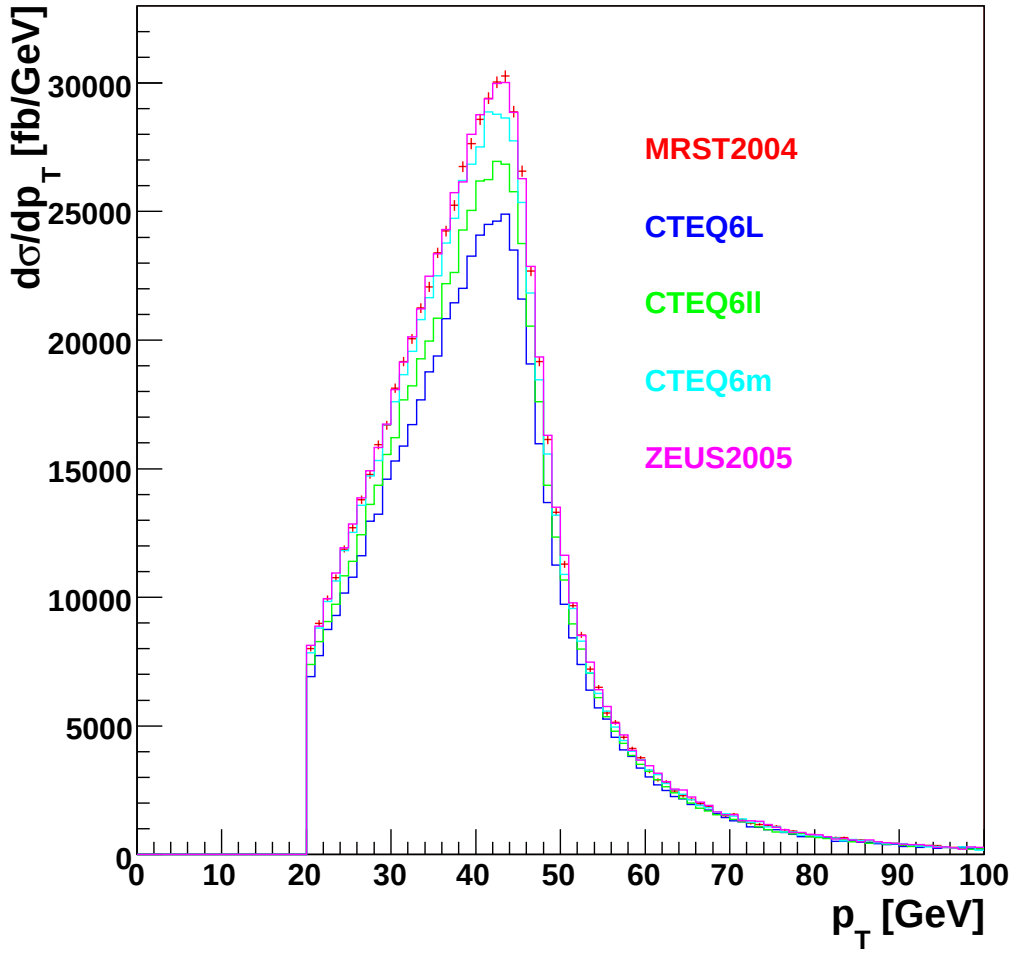

Figure 8.4: Differential cross section as a function of transverse momentum of electrons after Z cuts(Herwig/Jimmy). Five PDF sets are compared. The distributions for positrons are almost identical.

8.6 Kinematic characteristics of the Drell-Yan Z boson

The invariant mass distribution of Z is shown in Fig. 8.7 for CTEQ6ll and

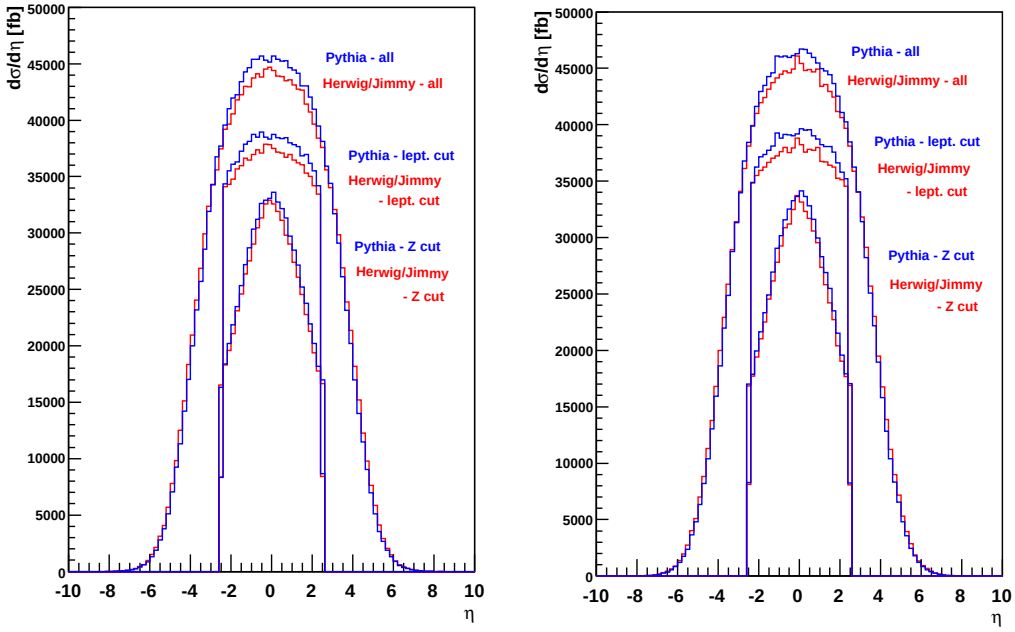

Figure 8.5: Differential cross section as a function of pseudorapidity of electrons (on the left) and positrons (on the right). CTEQ6ll parton distribution function was used for both generators.

Herwig. Histogram was fitted by Breit-Wigner distribution.

The peak for decayed Z after cut is broader due to the final-state radiation of e^-,e^+ and is shifted slightly to the left. The parameters of the fitting for all PDFs and both of generators are in Table 8.3.

The values of mass and width of Z approximatelly correspond to the tabulated values [2]: m = 91.1876 ± 0.0021 GeV and Γ = 2.4952 ± 0.0023 GeV. The high value of the χ^2/ndP for decayed Z is caused by final-state radiation that violated Breit-Wigner character of the mass distribution.

The mass distributions for all PDFs are shown in Fig. 8.8. Character of the distributions is almost identical with respect to the normalization, see Fig. 8.1.

The Z p_T distributions are shown in the Fig. 8.9 for CTEQ6ll PDF for Herwig and Pythia. There is very strong difference between them. Herwig

Table 8.3: Mean values of mass and width of the Z boson.

	all generated Z		
	mass [GeV]	**Γ [GeV]**	**χ^2/ndP**
Pythia			
CTEQ6ll	91.153 ± 0.002	2.485 ± 0.006	21.49/17
Herwig/Jimmy			
CTEQ6ll	91.197 ± 0.002	2.524 ± 0.006	17.68/17
CTEQ6L	91.197 ± 0.002	2.517 ± 0.006	20.81/17
CTEQ6m	91.200 ± 0.002	2.511 ± 0.006	26.52/17
MRST2004	91.196 ± 0.002	2.505 ± 0.006	11.88/17
ZEUS2005	91.198 ± 0.002	2.502 ± 0.006	26.24/17

	generated Z after cut		
	mass [GeV]	**Γ [GeV]**	**χ^2/ndP**
Pythia			
CTEQ6ll	91.167 ± 0.003	2.485 ± 0.009	16.01/17
Herwig/Jimmy			
CTEQ6ll	91.216 ± 0.003	2.530 ± 0.010	16.37/17
CTEQ6L	91.213 ± 0.003	2.527 ± 0.010	24.77/17
CTEQ6m	91.212 ± 0.003	2.512 ± 0.009	11.55/17
MRST2004	91.212 ± 0.003	2.508 ± 0.009	8.54/17
ZEUS2005	91.216 ± 0.003	2.509 ± 0.009	13.1/17

	decayed Z after cut		
	mass [GeV]	**Γ [GeV]**	**χ^2/ndP**
Pythia			
CTEQ6ll	90.947 ± 0.004	2.821 ± 0.012	469/17
Herwig/Jimmy			
CTEQ6ll	90.989 ± 0.004	2.875 ± 0.013	359.5/17
CTEQ6L	90.992 ± 0.004	2.878 ± 0.013	357.8/17
CTEQ6m	90.993 ± 0.004	2.868 ± 0.013	449.3/17
MRST2004	90.992 ± 0.004	2.862 ± 0.012	508.3/17
ZEUS2005	90.991 ± 0.004	2.872 ± 0.013	475.6/17

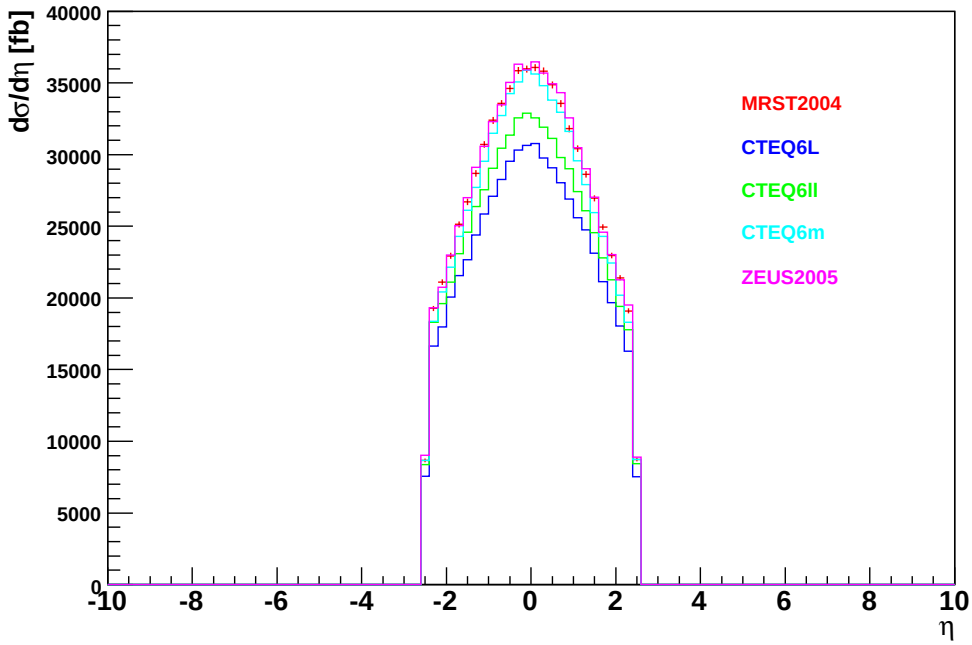

Figure 8.6: Differential cross section as a function of pseudorapidity of electrons after Z cuts. Five PDF sets are compared. The distributions for positrons are almost identical.

predicts higher cross sections in the area of $p_T < 15$ GeV compared to Pythia and vice versa in the area of $p_T > 15$ GeV. Numerically it is described in the Table 8.4.

The comparison of different PDFs is in Fig. 8.10. Their differences are fully explained by normalization, see Fig. 8.1. The mean values of p_T are in Table 8.5. The different shape of Pythia distribution is clearly manifested.

Fig. 8.11 shows rapidity distributions for CTEQ6ll PDF using Herwig and Pythia generator. Herwig predicts slightly wider peaks.

The comparison of rapidity distributions for all sets of PDFs using Herwig generator is displayed in Fig. 8.12. Differences are only in normalization.

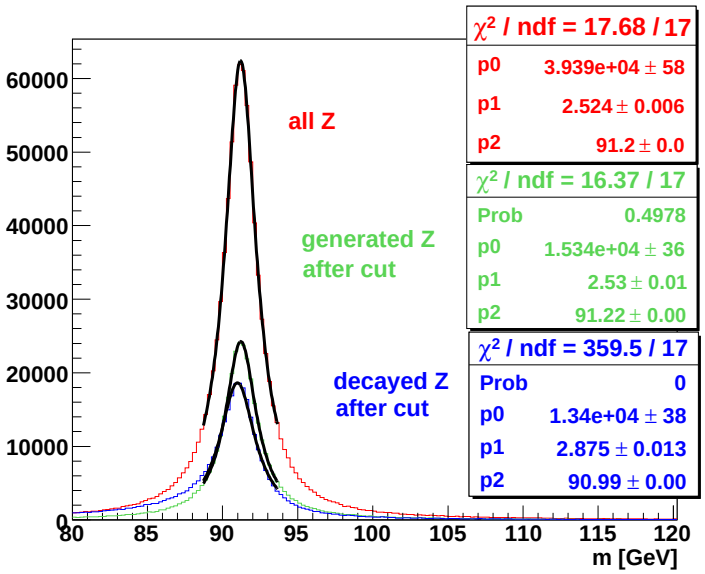

Figure 8.7: Distribution of invariant mass of Z boson on three different levels for CTEQ6ll PDF using Herwig/Jimmy generator. All lines are fitted by Breit-Wigner distributions and their characteristics are added.

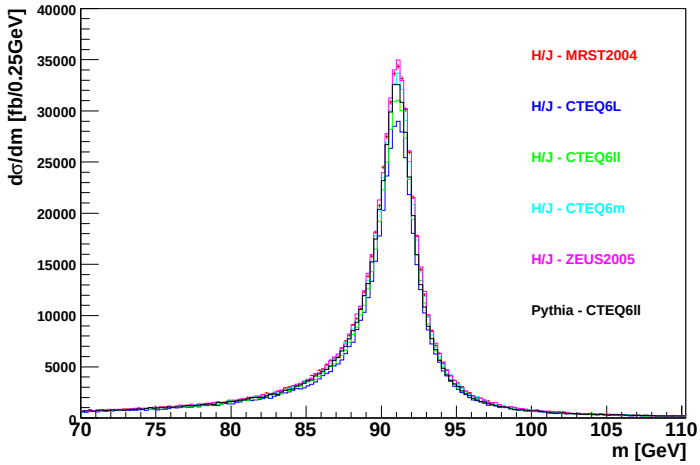

Figure 8.8: Differential cross section as a function of invariant mass of decayed Z boson after cuts for all PDFs using different generators.

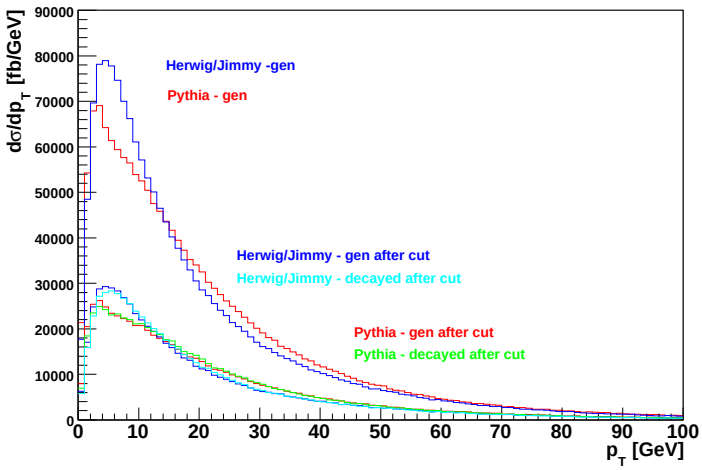

Figure 8.9: Differential cross section as a function of transverse momentum of Z boson on three different levels. CTEQ6ll PDF was used for different generators.

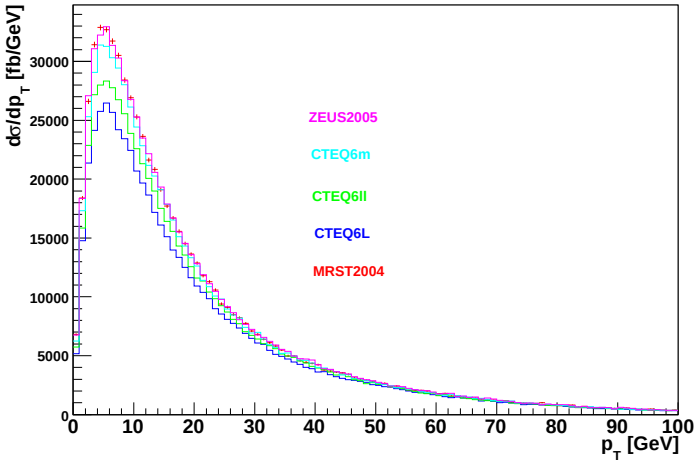

Figure 8.10: Differential cross section as a function of transverse momentum of Z boson for different PDFs using Herwig/Jimmy generator.

Table 8.4: Cross sections in the regions of transverse momentum of Z boson.

	Pythia: σ $[\mathbf{10^5}fb]$		**Herwig/Jimmy:** σ $[\mathbf{10^5}fb]$	
	$\mathbf{p_T < 15}$ **GeV**	$\mathbf{p_T > 15}$ **GeV**	$\mathbf{p_T < 15}$ **GeV**	$\mathbf{p_T > 15}$ **GeV**
all Z	8.056	8.754	8.933	7.777
gen. Z after cut	3.100	3.570	3.362	3.108
dec. Z after cut	3.071	3.599	3.323	3.147

Table 8.5: The mean values of p_T of Z and RMS for all PDFs.

	all generated Z		**generated Z after cut**	
	$\bar{p_T}$ **[GeV]**	**RMS [GeV]**	$\bar{p_T}$ **[GeV]**	**RMS [GeV]**
Pythia				
CTEQ6ll	21.27	19.00	21.97	19.52
Herwig/Jimmy				
CTEQ6ll	19.73	18.49	20.39	18.99
CTEQ6L	20.06	18.75	20.71	19.23
CTEQ6m	19.39	18.37	20.39	18.99
MRST2004	19.09	18.24	19.79	18.81
ZEUS2005	19.20	18.35	19.99	18.94

	decayed Z after cut	
	$\bar{p_T}$ **[GeV]**	**RMS [GeV]**
Pythia		
CTEQ6ll	21.92	19.19
Herwig/Jimmy		
CTEQ6ll	20.38	18.65
CTEQ6L	20.70	18.90
CTEQ6m	20.38	18.65
MRST2004	19.83	18.50
ZEUS2005	20.02	18.64

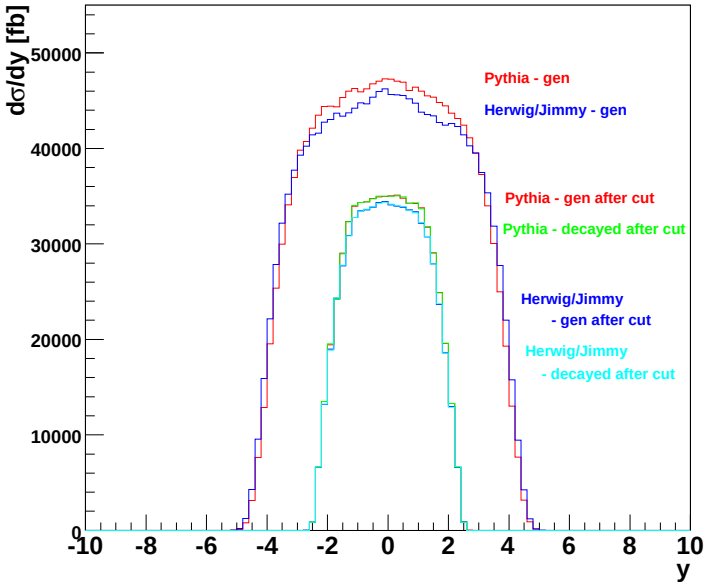

Figure 8.11: Differential cross section as a function of rapidity of Z boson on three different levels for CTEQ6ll PDF using Herwig/Jimmy and Pythia generators.

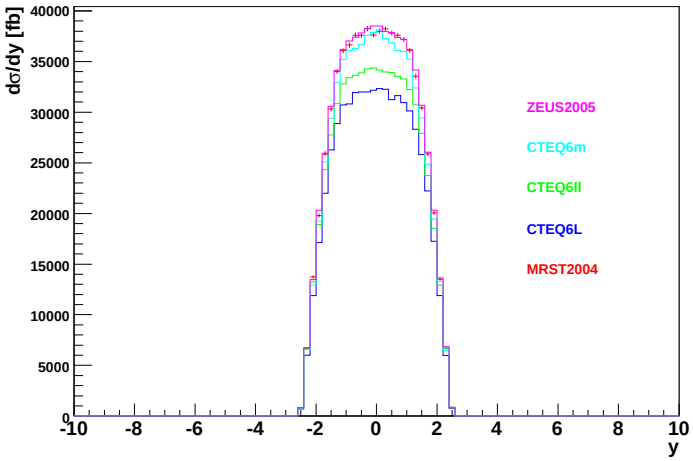

Figure 8.12: Differential cross section as a function of rapidity of decayed Z boson after cut for different PDFs using Herwig/Jimmy generator.

The distributions of fraction x_a are shown in Figures 8.13 and 8.14. The first one compares Pythia and Herwig generators and describes the influence of cut. The Z cut dramatically decrease the range of magnitude of x_a. Fig. 8.14 shows almost identical distributions for all PDFs.

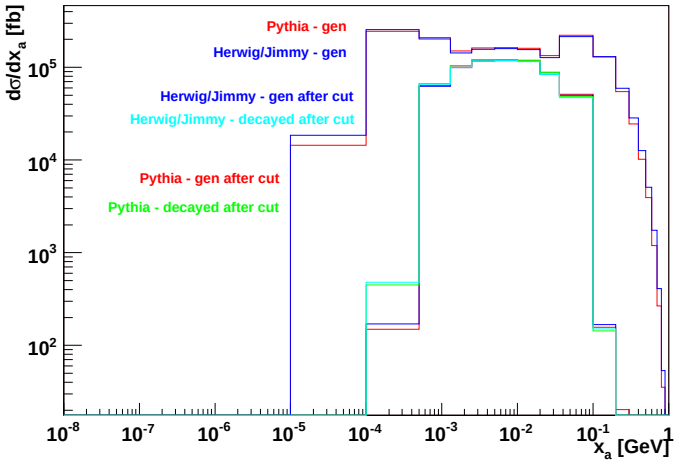

Figure 8.13: Differential cross section as a function of the fraction x_a on three different data levels for CTEQ6ll PDF using Herwig/Jimmy and Pythia generators.

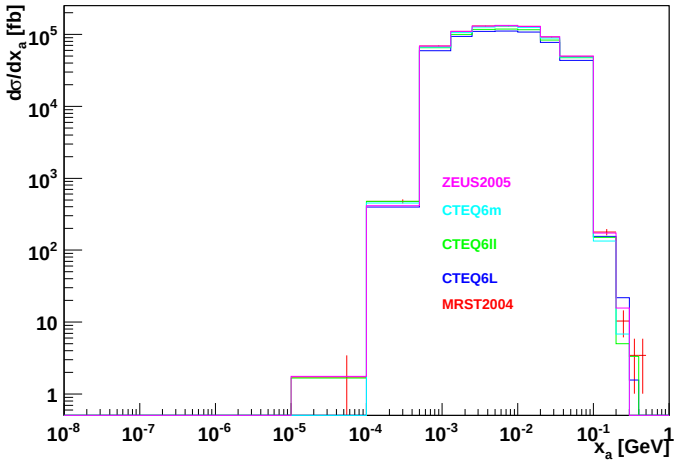

Figure 8.14: Differential cross section as a function of the fraction x_a for the Z boson decay after cut for different PDFs using Herwig/Jimmy generator.

8.7 P_T distribution of Z boson in x_a bins

CTEQ6ll PDF was used for demonstration of differential cross sections depending on transverse momentum of decayed Z boson after cut in seven x_a bins covering the whole x_a scale, see Fig. 8.15. The p_T distributions seems to depend only on normalization, the shape of lines does not depend on the chosen bin of x_a.

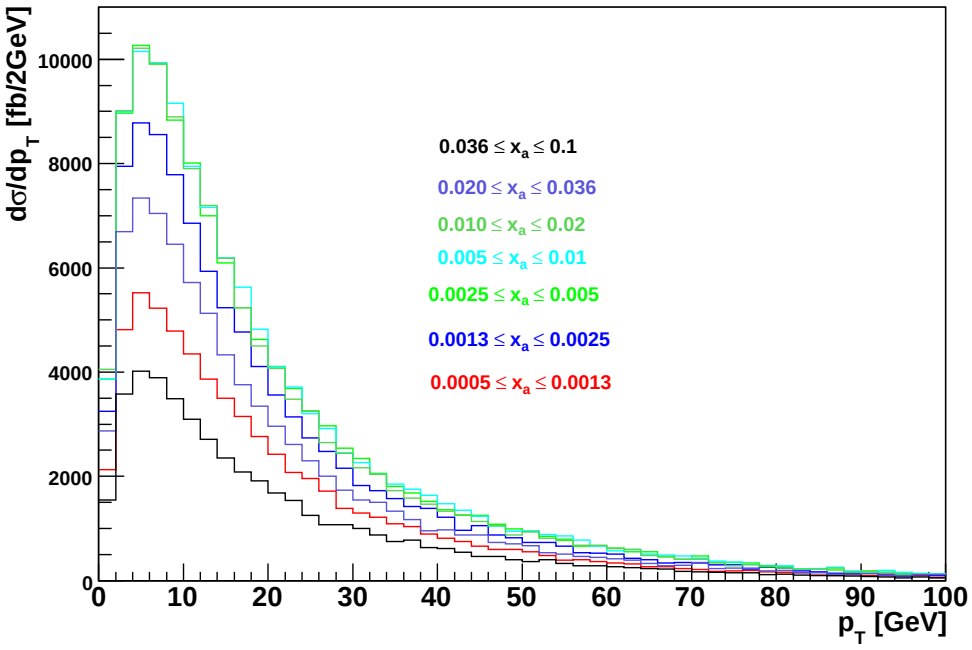

Figure 8.15: Differential cross section as a function of transverse momentum of decayed Z boson after cut in different x_a-bins for CTEQ6ll PDF using Herwig/Jimmy generator.

Chapter 9

Summary and conclusions

Kinematic characteristics of the Z boson and its secondaries created in the process $pp \rightarrow X + Z \rightarrow e^{-}e^{+}$ at 14 TeV were studied on the generator level.Two generators were used - Herwig/Jimmy and Pythia. Five different event sets were generated with Herwig/Jimmy. They differ only in PDF. The following PDFs were used: CTEQ6ll(used also in Pythia),CTEQ6L, CTEQ6m, MRST2004 and ZEUS2005. The first three are leading order PDFs, the last two are next-to-leading order ones.

The expected multiplicity of Drell-Yan Z decayed in $e^{-}e^{+}$ channel are 3.27 $\times$ 10^5, 10^6, 10^7 for the integrated luminosity 1, 10 and 100 fb^{-1}, respectively for events generated with Pythia. These numbers differ from 3.17 $\times$ 10^5, 10^6, 10^7 generated with Herwig/Jimmy using the same PDF set by about 3.2%. The identification and reconstruction efficiency is supposed to be 70 % for the electrons and positrons with $p_T > 20GeV$ and $|\eta| < 2.5$. Other detector effects and background corrections are not taken into account.

Herwig/Jimmy event generator was used for comparison of different sets of PDFs. The expected multiplicities are 2.96 $\times$ 10^5, 3.17 $\times$ 10^5, 3.40 $\times$ 10^5, 3.48 $\times$ 10^5 and 3.50 $\times$ 10^5 for integrated luminosity 1 fb^{-1}. They correspond to CTEQ6L, CTEQ6ll, CTEQ6m, MRST2004 and ZEUS2005 PDF sets.

No strong dependence on the PDF used was found for the p_T and η distributions of secondary leptons. The pseudorapidity distribution obtained with Herwig/Jimmy is wider compared with the Pythia one.

The distributions of Z invariant mass for different PDFs are almost identical and differ only in normalization. The same is true for the distributions of rapidity, transverse momentum and x_a.

As to the comparison of distributions of kinematic characteristics of Z

obtained with Herwig/Jimmy and Pythia, the following was found. The Z invariant mass and x_a distributions are quite similar. The rapidity distribution of Z obtained with Herwig/Jimmy is wider than the Pythia one. The difference of the Z transverse momentum distributions is dramatic. The Herwig distribution is significantly shifted to the lower values. The Z transverse momentum distributins were created in seven roughly equally populated x_a bins. The Herwig/Jimmy events with CTEQ6ll were used for this purpose. No strong dependence on x_a bins was found.

Chapter 10

References

[1] Francis Halzen, Alan D. Martin, Quarks and leptons:An introductory course in modern particle physics, John Wiley & Sons Inc. New York,USA, 1984

[2] S. Eidelman et al.,Rewiev of particle physics, Physics Letters B 592, Issues 1-4, 2004

[3] Jiří Hořejší, Fundamentals of Elektroweak Theory, Karolinum, Praha, 2002

[4] Jiří Chýla, Quarks, partons and Quantum Chromodynamics, *http* : *//www − hep.fzu.cz/Theory/notes/text.pdf*

[5] W.Greiner, B.Mueller, Quantum Chromodynamics, Springer-Verlag, Berlin, 2001

[6] Jianwei Qiu, Xiaofei Zhang, Phys. Rev. D 63, 114011 (2001)

[7] Y.L.Dokshitzer, D.I.Diakonov, and S.I.Troyan, Phys. Rep. 58, 269 (1980)

[8] G.Parisi and R.Petronizio, Nucl. Phys. B154, 427 (1979)

[9] J.C.Colins, D.E.Soper, and G.Sterman, Nucl. Phys. B250, 199 (1985)

[10] G. Corcella, I.G. Knowles, G. Marchesini, S. Moretti, K. Odagiri, P. Richardson, M.H. Seymour and B.R. Webber, HERWIG 6: an event generator for Hadron Emission Reactions With Interfering Gluons (including supersymmetric processes)*, JHEP 0101 010, 1-91, 2001

[11] T. Sjoestrand, L. Loennblad, S. Mrenna, P. Skands, Pythia 6.2, Physics and Manual, hep-ph/0108264, LU TP 01-21, 2002

[12] L.W.Whitlow, E.M.Riordan, S.Dasu, S.Rock, and A.Bodek, Physics Letters B 282, 475-482 (1992)

[13] BCDMS Collaboration, Physics Letters B 223 (1989)

[14] The ZEUS Collaboration, Eur. Phys. J. C21, 443-471 (2001)

[15] The NMC Collaboration, Nuc. Phys. B 483, 3-43 (1997)

[16] Fermilab E665 Collaboration, Physical Review D 54 (1996)

[17] The H1 Collaboration, Eur. Phys. J. C 30, 1-32 (2003)

[18] The H1 Collaboration, Eur. Phys. J. C 21, 33-61 (2001)

[19] G. Corcella, I.G. Knowles, G. Marchesini, S. Moretti, K. Odagiri, P. Richardson, M.H. Seymour and B.R. Webber, HERWIG 6.5 Release Note, hep-ph/0210213, 1-7, 2002

[20] T. Sjoestrand, P. Eden, C. Friberg, L. Loennblad, G. Miu, S. Mrenna and E. Norrbin High-energy-physics event generation with Pythia 6.1, Computer Physics Commun., 135, 238, 2001

[21] W. Giele, M.R. Whalley, LHAPDF version 4.1 Users Guide, *http* : *//hepforge.cedar.ac.uk/lhapdf/manual*

[22] Ruediger Voss, CERN-PPE-92-044, 1992

[23] ATHENA, http://atlas.web.cern.ch/atlas/GROUPS/SOFTWARE/OO/architecture/

[24] ROOT, http://root.cern.ch